frontiers | Frontiers in Earth Science

TYPE Original Research
PUBLISHED 09 May 2023
DOI 10.3389/feart.2023.1106690

OPEN ACCESS

EDITED BY
Amr Deaf,
Assiut University, Egypt

REVIEWED BY
Mahmoud Leila,
Mansoura University, Egypt
Walaa Awaad Awaad Ali,
Matrouh University, Egypt

*CORRESPONDENCE
Xin Cui,
cuixin8868@163.com

RECEIVED 24 November 2022
ACCEPTED 17 April 2023
PUBLISHED 09 May 2023

CITATION
Cui X, Li J, Jiang H, Yan H and Qi Q (2023), Hydrocarbon potential assessment of the lacustrine fan delta reservoirs in the Lower Cretaceous syn-rift Xing'anling Formation in the Beier Sag, Hailar Basin, Northeast China.
Front. Earth Sci. 11:1106690.
doi: 10.3389/feart.2023.1106690

Hydrocarbon potential assessment of the lacustrine fan delta reservoirs in the Lower Cretaceous syn-rift Xing'anling Formation in the Beier Sag, Hailar Basin, Northeast China

Xin Cui[1,2]*, Jianghai Li[2], Hongfu Jiang[3], Hongxing Yan[4] and Qingpeng Qi[5]

[1]National Key Laboratory of Remote Sensing Information and Image Analysis Technique, Beijing Research Institute of Uranium Geology, CNNC, Beijing, China, [2]Institute of Oil and Gas, School of Earth and Space Sciences, Peking University, Beijing, China, [3]CNPC Hailar Exploration and Development Administration, Daqing Oilfield Company, Daqing, China, [4]CNPC Institute of Liaohe Oilfield, Panjin, China, [5]CNPC Institute of Geology, Shuguang Oil Production Plant of Liaohe Oilfield Company, Panjin, China

Efficient exploration and development of oil and gas resources in complex geological environments continue to pose significant challenges for the energy industry. The localization and extraction of reservoirs in basins with complex structures, developed faults, and scattered sedimentary sand bodies are topics of international interest. One such basin, the Hailar Basin in northeastern China, represents a complex geological environment with heterogeneous distributions of oil and gas reserves, along with variable reservoir conditions, leading to challenges in hydrocarbon exploration and extraction. The Sudeert oil field, situated within this basin, is known for its high productivity; nevertheless, the underlying factors responsible for its success are not yet fully comprehended. Based on seismic, logging, and core data from the Sudeert oil field, as well as previous research, this study comprehensively analyzed the sedimentary environment, sedimentary facies characteristics, sand body distribution patterns, vertical stacking relationships of sand bodies, and hydrocarbon accumulation potential of the oil reservoirs in the Lower Cretaceous Xing'anling Formation in the Sudeert oil field. The Xing'anling Formation I and II oil reservoirs are deposited in a fan-delta front sedimentary environment, and the sedimentary microfacies that are conducive to the development of reservoir sand bodies include underwater distributary channels, underwater natural levees, estuary dams, front silt beds, and turbidite sands. Among them, the underwater distributary channel microfacies is the main depositional facies for the development of reservoir sand bodies. Three major depositional patterns of fan lobes can be identified within this depositional system: 1) isolated, 2) contact, and 3) superimposed lobes. Different combinations of lobes developed in different blocks and resulted in different sand body depositional patterns. The isolated lobes mainly developed in the western oil-producing (B28 block) due to the scarcity of sand and slowly increasing accommodation space. The contact lobes mainly developed in the central oil-producing block (B14 block) due to sufficient sediment supply and steadily increasing accommodation space across a wide area. The superimposed lobes mainly developed in the southeast oil-producing

block (B16 block) due to sufficient sediment input and steadily increasing accommodation space within a restricted area. In the whole study area, the superimposed lobe pattern is the most favorable depositional pattern and forms the highest-quality reservoirs because of the high degree of sand body connectivity. These results also highlight the utility of sedimentary patterns and sand body assemblage studies for the oil exploration and development of similar rifted basins.

KEYWORDS

Hailar basin, Lower Cretaceous Xing'anling formation, sedimentary environment, lacustrine fan delta reservoirs, sand body distribution patterns, depositional patterns, hydrocarbon accumulation potential, oil and gas exploration

1 Introduction

The demand for oil and gas resources in modern society is steadily increasing. However, discovering and exploiting these resources is a complex and challenging task that requires an understanding of the geological conditions of the hydrocarbon basin. As an important hydrocarbon basin, rift basins have naturally become a focus in the search for oil and gas resources. The patterns of sand deposition in northeastern Asian rift basins such as the Hailar, Erlian, Songliao, and Bohai basins are of both academic and industrial interest (Lin et al., 2001; Morley, 2002; Ren et al., 2002; Dou and Chang, 2003; Lin et al., 2004; Feng et al., 2010) because the basins include prolific oil and gas fields. The basins formed during back-arc rifting in the Mesozoic–Cenozoic and are infilled with several kilometers of alluvial and lacustrine siliciclastic deposits (Allen et al., 1997). In extensional basins, the spatial distribution of reservoirs is a primary control on hydrocarbon recovery (Valencia, 1989; Lin et al., 2001; Morley, 2002; Ren et al., 2002; Dou and Chang, 2003; Lin et al., 2004; Feng et al., 2010) and rift-related faults control the rate and style of accommodation creation and sand dispersal (Folk, 1954; Ryder et al., 1976; Patton et al., 1994; Jia et al., 2014; Zhou et al., 2014).

The Hailar Basin, located in the western region of northeast China (Figures 1A, B), is one of the most important petroliferous basins in the Daqing exploration area (Wang, 2019). The Hailar Basin is estimated to have 8.50×10^8 tons of oil resources. These reservoirs are predominantly conventional oil and gas, with structural reservoirs the most common type, followed by fault-block-lithology reservoirs (Li, 2021). By the end of 2018, the proven oil reserves comprised 1.63×10^8 tons, with approximately 6.57×10^8 tons yet to be discovered (Wang, 2019). Therefore, the Hailar Basin is a new strategic area of oil and gas resources in the Daqing oil field. The Beier Sag is located in the southern part of the Hailar Basin and is a secondary tectonic unit of the basin, which is a part of the first-order tectonic unit, the Beier Lake Depression (Figure 1C). The Beier Sag has exploratory potential for oil and gas (Zhang et al., 2012), with an area of 2,166 km^2 (Fu et al., 2012). The Sudeert fault zone, located in the Beier Sag (Figure 1D), is one of the most important hydrocarbon-producing areas in the Hailar Basin (Wang et al., 2007; Feng et al., 2011). It is a fault zone between the oil-rich Beizhong Sag and Beixi Sag. The fault zone was cut by numerous NE- and near EW-trending normal faults and formed dozens of complex fault blocks of different sizes. In-plane, it is characterized by belts in the S-N direction and blocks in the E-W direction (Figures 1, 2).

Reservoir rocks consist of syn-rift fluvial and deltaic sandstones (Xu et al., 2008b; Zhou et al., 2014) including those in the Lower Cretaceous Xing'anling Formation. The reservoir units in the Xing'anling Formation are heterogeneous and laterally variable, which makes detailed correlations difficult. No systematic analysis of this depositional system has previously been performed and depositional settings are poorly understood. The Hailar Basin is a complex faulted continental sedimentary basin in north-eastern China, consisting of a series of graben basin groups. Compared with conventional rift-type sedimentary basins, the Hailar Basin has more complex structures and sedimentary evolution processes. The oil and gas accumulation units in these types of basins have characteristics such as developed fractures, broken fault blocks, and narrow distributions of reservoirs, making oil and gas exploration more challenging. As oil and gas exploration goes deeper, oil and gas resources in sedimentary basins with simpler structures are being exploited. Oil and gas resources concentrated in complex fault block reservoirs, deep tight sandstone reservoirs, or basement fault zones, are the focus of future oil and gas exploration. Our study focused on the Sudeert oil field in the Hailar Basin, a typical complex faulted oil field, and aimed to provide insights into addressing the challenges of oil and gas exploration and development in complex faulted sedimentary basins. By analyzing information from various data sources such as regional seismic, logging, and core data, this study investigated the regional tectonic environment, sedimentary system, reservoir distribution characteristics, and oil and gas reservoir control factors. We also discussed the use of abundant technical methods and geological data to tap into the oil and gas resources in such basins. These findings not only benefit the exploitation of oil and gas resources in China but also provide valuable insights into similar oil and gas resource basins worldwide, such as the Texas Basin, the Gulf of Mexico Basin, and the Alberta Basin.

1.1 Geological setting

The Hailar Basin in northeastern China is a complex Upper Jurassic–Cretaceous rift basin (Chen et al., 2007; Feng et al., 2011; Sun et al., 2011; Cui et al., 2016) (Figures 1–3) and is similar in terms of structure to the larger-scale Erlian and Songliao Basins (Traynor and Sladen, 1995; Wu et al., 2006; Zhou et al., 2014; Li et al., 2015).

The Hailar Basin includes the hydrocarbon-rich Wuerxun and Beier Sags (Sun et al., 2011; Zhang et al., 2012; Li et al., 2015) which cover areas of ~2,240 km^2 and ~3,010 km^2, respectively. In the Beier

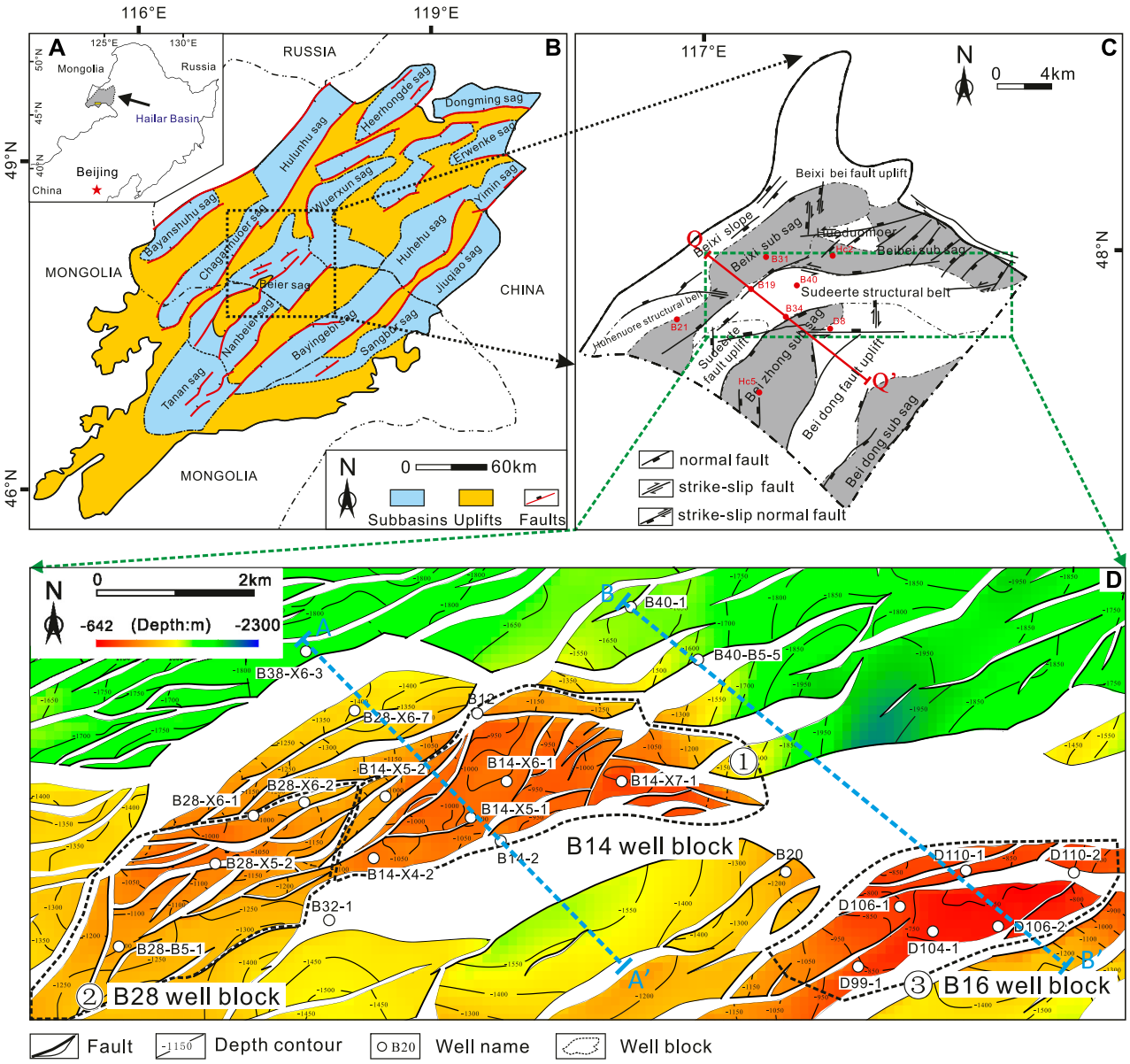

FIGURE 1
Map showing the location of the study area. **(A)** Hailar Basin. **(B)** Tectonic units of the Hailar Basin. **(C)** Tectonic units of the Beier Sag. Green box, area of 3D seismic data and acoustic impedance attribute slices used in the study. **(D)** Structural contour map of T4 seismic reflector (corresponding to the top of the Xing'anling Formation). Blue dotted lines (AA' and BB'), locations of well-seismic correlation sections and tectonic evolution profiles used in this study. The two sections were also used to predict the vertical distribution characteristics of the sand bodies.

Sag, the Sudeert fault zone (Figure 1C) hosts the Sudeert oil field and is an important hydrocarbon-producing area (Feng et al., 2010; Cui et al., 2016). The NE-SW trending Sudeert fault zone is located in the center of the Beier Sag between the Beixi and Beizhong sub-sags (Figure 1C) and covers an area of 150 km^2 with multiple fault-bound structural blocks with variable orientations (Figure 1D) (Lin et al., 2008; Wang et al., 2012). The fault zone can be divided into a central fault belt, northern fault terrace, eastern fault terrace, and western fault scarp (Figure 1D). This study focuses on the central fault belt and western fault scarp, which have been divided into three blocks named after the wells (Figure 1D), B28, B14, and B16, from west to east (Kang et al., 2008; Wang et al., 2012).

The basement of Beier Sag is composed of Upper Palaeozoic and Lower Mesozoic granites and Jurassic metamorphic rocks (Chen et al., 2007; Zhou et al., 2014; Yi et al., 2015). The unconformably overlying sedimentary cover is dominated by a Lower Cretaceous succession comprising the Xing'anling (K1x), Nantun (K1n), Damoguaihe (K1d), and Yimin (K1y) Formations (Figure 3). The Xing'anling Formation is in general 100–590 m thick in the Sudeert fault zone and is composed of non-marine siliciclastics from conglomerates through to mudstones (Figure 3) (Wang et al., 2012). Xing'anling Formation is in unconformable contact with the metamorphic rock strata of the Budate Formation at the base. The top also shows a surface with regional unconformity between

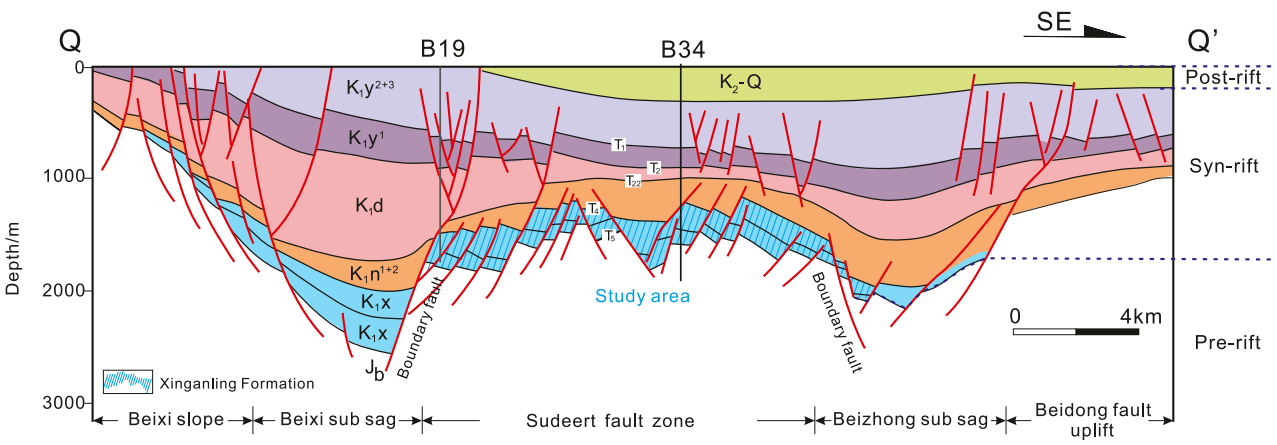

FIGURE 2
Cross section (location marked in Figure 1, QQ') showing the various tectonic structural zones and key stratigraphic intervals within the Beier Sag. Blue shaded area, study area. Modified from Sun et al. (2011).

the Nantun and Xing'anling Formations. Previous studies (Xu et al., 2008a; Wang et al., 2012) divided the Xing'anling Formation into four members, numbered (from youngest to oldest) 1, 2, 3, and 4 (Figure 4A). Members 1 and 2 in the upper part of the Xing'anling Formation are the most important oil-producing units in the Sudeert oil field (Figure 4). Both members are dominated by sandstones and sandy conglomerates with some tuffs; Member 1 is ~10–250 m thick, while Member 2 is ~20–150 m thick. Member 3 contains sandy conglomerates and fine and coarse sandstones and is ~40–200 m thick, with volcaniclastic rocks including rhyolitic tuffs. Member 4 is ~150–800 m thick and composed of sandy conglomerates and breccias with some shales. Based on well correlations (Figure 4B), Members 1 and 2 were present in blocks B28, B14, and B16 with relatively consistent thicknesses. The deposit thicknesses of Members 1 and 2 of well block B16 were the largest, and the thickness decreased gradually to well block B28 (Figure 4B).

Pre-rift (pre-Cretaceous), syn-rift (Early Cretaceous), and post-rift (Late Cretaceous) phases are recognized in the Beier Sag (Sun et al., 2011; Zhou et al., 2014; Liu et al., 2015), with corresponding early extensional, later oblique-extensional, and late-stage inverted faults (Sun et al., 2011; Figure 2). During the early Cretaceous period in the Xing'anling Formation, the Beier Sag experienced a north-eastward right-lateral extensional, rotational, wrenching, and faulting movement. During this time, the mountains on both sides of the Hailar Basin rose quickly, and sediment accumulated rapidly within the basin, consisting mainly of coarse debris from nearby and multiple sources, forming a set of fan delta sediments. Later (Nantun Formation), the water bodies in various faulted basins deepened and expanded, and the sedimentation was mainly dominated by gravity flows, resulting in nearshore fans, turbidite fans, and fan delta sediments. In the middle and late early Cretaceous period (during the development of the Damoguaihe and Yimin Formations), the basin entered a rapid subsidence stage dominated by shallow lacustrine sedimentation. In the late Cretaceous period (Qingyuangang Formation), the basin entered a shrinking and dying stage of subsidence with the sedimentation mainly dominated by deep and semi-deep lacustrine sedimentary facies (Kang et al., 2013).

2 Data and methods

The data used in this study include cores (conventional cores, with sampling intervals of <0.2 m), seismic dataset (a three-dimensional SEGY data type, covering an area of 406 km^2, with a main research area of approximately 150 km^2), wireline logs, seismic attribute slices, and inversion sections (Figure 5). Over 200 boreholes have been drilled in blocks B14, B28, and B16 in the Sudeert fault zone, and production test data were made available by the Daqing Oil Company, Ltd. Approximately 965 m of core from 30 wells were described, and samples from 18 wells were analyzed to interpret the depositional environments. We evaluated different sedimentary facies markers and subsequently divided the sedimentary microfacies by observing the rock cores (color characteristics, stratigraphic structures, fossil features), consulting internal drilling geological reports on the oil field (e.g., mineral analysis data), and analyzing the sedimentary phase characteristics reflected by the logging curves corresponding to the depths of the rock cores (Zhao and Cui, 2014). Seismic data and isopach maps of sand bodies were also used to assist in the interpretation of the depositional environments.

The detection parameters for the core porosity mainly consisted of the total and effective porosities under conventional conditions, measured by gas detection and kerosene saturation methods using a CMS-300 fully automatic core analyzer. This was primarily used to evaluate the reservoir's storage capacity. The permeability was also measured using the fully automatic analyzer, under conventional conditions, using the air permeability method, primarily to evaluate the connectivity of the pore spaces in the reservoir. The TOC values were primarily derived from geological data from within the oil field.

Structural and stratigraphic interpretations of the Xing'anling Formation were based on an analysis of a 3D seismic dataset covering an area of 150 km^2 (green box in Figure 1B). The workflow for seismic interpretations included the tops and bottoms

10.3389/feart.2023.1106690

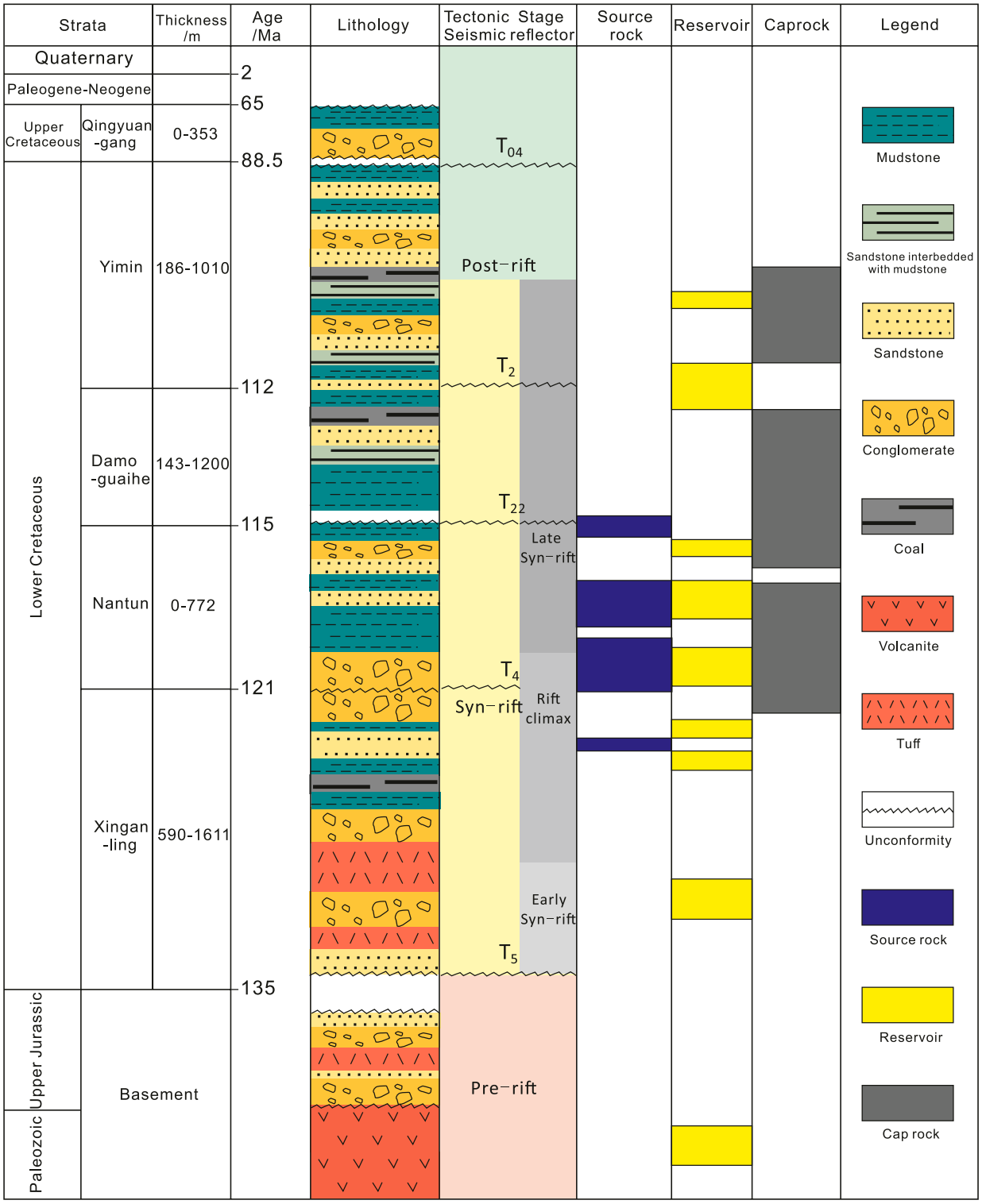

FIGURE 3
Comprehensive geological histogram of the Sudeert fault zone, Hailar Basin (modified after Wang et al., 2012).

of Members 1–4, including calibration, synthetic seismogram, well-tie seismic cross-section contrasting and compartmentalizing, member reflector tracking and fault interpretation, and inspection of the seismic interpretation results (Figure 5).

The amplitude attribute can well reflect the system of fluvial-lacustrine deposition in the study area. The strong acoustic impedance reflects sand-rich deposition, while weak acoustic impedance reflects mud-rich deposition (Morozov and Ma,

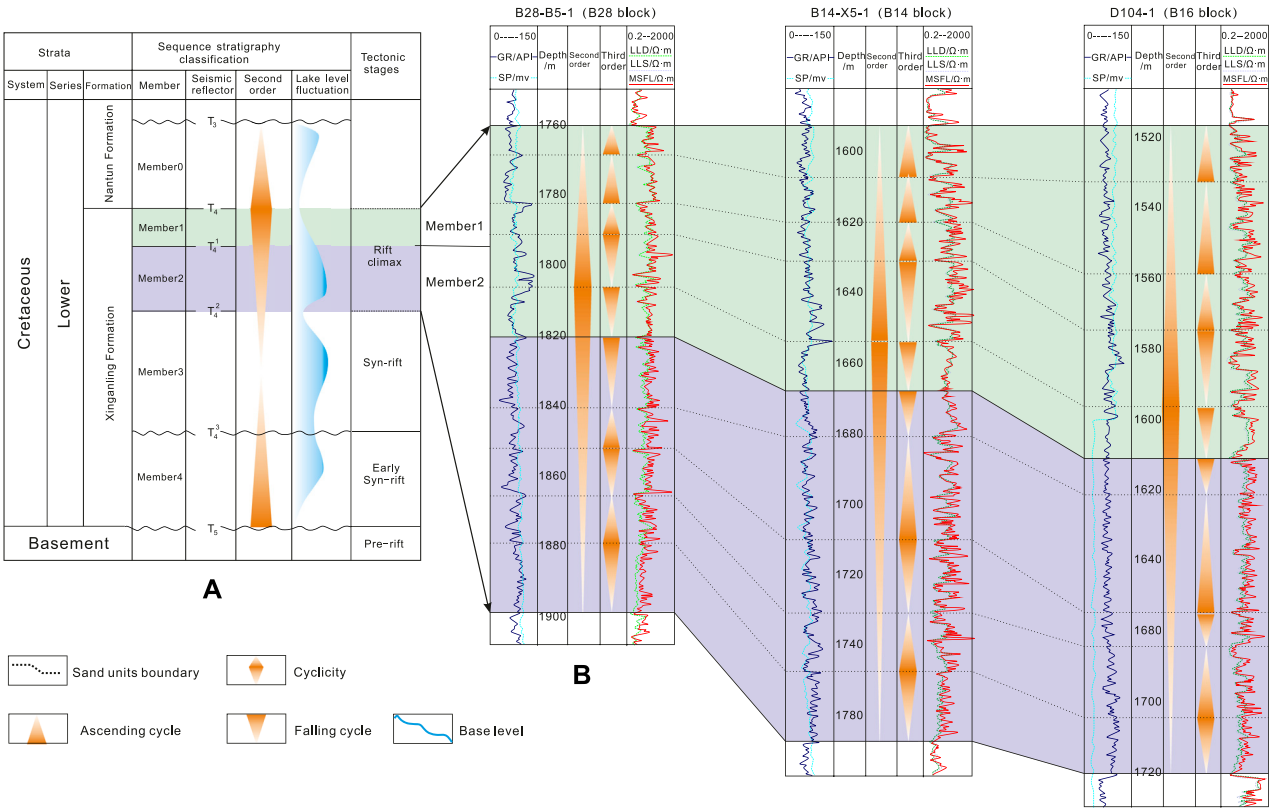

FIGURE 4
(A) Generalized stratigraphic column of the Lower Cretaceous strata of the Sudeert fault zone, Hailar Basin. **(B)** Borehole correlation profiles showing the thickness variations in Members 1 and 2 in well blocks B28, B14, and B16. The well locations are shown in Figure 1.

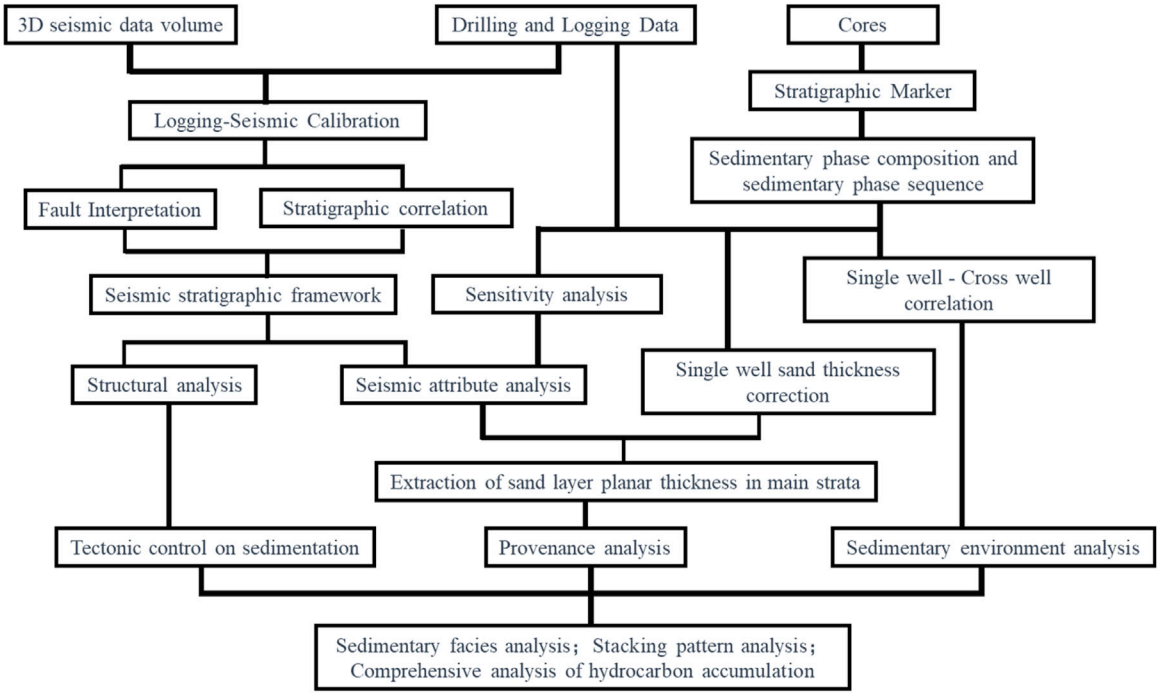

FIGURE 5
Flowchart of the data and methodology used in this study.

TABLE 1 Porosity statistics for blocks B28, B14, and B16 of the Xing'anling Formation (the error values indicate standard error, the same as in the following tables).

	≤10	10<Φ<15	15≤Φ<25	25≤Φ<30
B28 block	92.0 ± 4.2	8.0 ± 1.5	0.0 ± 0.0	0.0 ± 0.0
B14 block	0.0 ± 0.0	30.9 ± 2.4	68.3 ± 2.8	0.8 ± 0.2
B16 block	1.4 ± 0.6	8.0 ± 1.5	60.6 ± 2.7	30.0 ± 2.5

TABLE 2 Permeability statistics for blocks B28, B14, and B16 of the Xing'anling Formation.

	K≤1	1<K≤10	10<K≤50	50<K≤100	100<K
B28 block	82.0 ± 3.5	8.0 ± 1.1	0.8 ± 0.2	0.0 ± 0.0	0.0 ± 0.0
B14 block	94.3 ± 2.1	8.0 ± 1.1	0.0 ± 0.0	0.0 ± 0.0	0.0 ± 0.0
B16 block	24.7 ± 1.2	30.9 ± 2.4	19.9 ± 2.0	4.9 ± 0.7	12.4 ± 1.3

2009). A strong amplitude corresponds to pro delta front deposition, a medium-weak amplitude corresponds to distal delta front lobe deposition, and a weak amplitude corresponds to semi-deep lake mudstone deposition. Seismic attribute slices are used widely for the lithological and petrophysical prediction of reservoirs (Chopra and Marfurt, 2006; Asim et al., 2016). The present study used acoustic impedance attribute slices (Figure 1B) from Members 1 and 2 of the Xing'anling Formation to investigate the characteristics of sand bodies in the Sudeert fault zone. In addition, two in-line inversion sections from blocks B14 and B16 (AA' and BB' in Figure 1D) were used to predict the vertical distribution characteristics of the sand bodies (c.f. Torres-Verdin et al., 1999). These two sections (AA' and BB' in Figure 1D) were also used for well-seismic profile comparisons and analysis of the tectonic evolution history.

By seismic sand body attribute inversion, the sand body inversion thicknesses of Members 1 and 2 were calculated. The sand body inversion thickness was corrected by the thickness obtained from the well logs in the study area; hence, the final thickness map of the sand body. The diagrams of deposition facies in the study area were mapped by combining the thickness map of the sand body, the seismic attribute slices, and single well facies.

3 Results

3.1 Data on core porosity and permeability

Visualization of the drill core data (nearly 100 core samples from 10 wells such as B14X-5-4, B14-X5-6, and D106-2; Members 1–4; Xing'anling Formation, blocks B14, B16, and B28) physical property analysis (Tables 1–4) showed that block B16 has the characteristics of medium-high porosity and low to ultra-low permeability reservoirs, block B14 block is characterized by high porosity and ultra-low permeability, and block B28 features low porosity and ultra-low permeability (Table 1). Excluding the influence of geological processes (e.g., cementation) on the later transformation of reservoir physical properties, the superposition relationships of the lobes and sand bodies of the three blocks also have some influence. The vertical stacking relationships of the sand bodies, indicated by the differences in physical property data from different well blocks and their geological implications for petroleum geology are further addressed in the Discussion section.

3.2 Facies types

Based on the cores of Members 1–4 of Xing'anling Formation from B14-X5-1, B14-X6-1, D106-1, and D110-2 (Figures 6, 7), the petrography and facies types of Lower Cretaceous Xing'anling Formation in the study area were identified according to type, texture, grain size, and sedimentary structure. The core descriptions showed that the lithofacies type of the fan-delta system is complex and includes three rock types (Miall, 1977).

3.2.1 Conglomerate lithofacies

Conglomerate lithofacies is the main lithofacies type in the study area (Figures 6C, E, F). This type is dominated by gravel clasts with sandy or muddy matrices and displays massive structures, cross-bedding, and normal grading.

The clast-supported conglomerates (Figure 6E) were dominated by moderate-well sorted granule-pebble to conglomerate and were clast-supported. The sedimentary structures were not well-developed in this lithofacies.

This lithofacies represented the tractive current deposits that developed in braided channels. The trough cross-bedding conglomerates (Figure 6C) were dominated by medium-well-sorted pebbles to granules. The matrix in this lithofacies was mainly gray sand. This lithofacies represented the tractive current deposits that developed in subaqueous distributary channels. Moreover, well-preserved plant fossils were found in the core of D106-1 (Member 1, depth 1,377.1 m) in block B16 (Member 1, depth 1,377.1 m) (Figure 6F), suggesting the sedimentary characteristics of near-source rapid accumulation in this area.

3.2.2 Sandstone lithofacies

The sandstone lithofacies mainly developed in the distal and late stages of the fan-delta system. The graded-bedding sandstones (Figure 6A) were dominated by fine-to-coarse-grained sands with normal grading. Sands in this lithofacies were light gray in color. This lithofacies represented high to low-density turbidity current deposits.

The trough cross-bedding sandstones (Figure 6B) were dominated by medium-to coarse-grained sands that are gray in color. This lithofacies represented tractive current deposits that developed in subaqueous channels. The massive sandstones (Figure 6D) were dominated by coarse to medium sands with little gravel. This lithofacies represented high-density turbidity currents. The massive conglomeratic medium-coarse sandstone was light gray in color. Conglomerates were observed at the top of the core (Figure 6D).

3.2.3 Mudstone lithofacies

The mudstone lithofacies were gray with no obvious sedimentary structure. This lithofacies represented semi-deep lake deposits connected to extremely weak hydrodynamics.

TABLE 3 Porosity and permeability statistics of typical wells in blocks B28 and B14 of the Xing'anling Formation.

Wells properties	B28 block		B14 block				
	B28	B28	B14	B14-X5-4	B14-X5-4	B14-X5-4	B14-X5-6
Permeability	8.6 ± 0.6	8.6 ± 0.6	14.8 ± 1.1	17.3 ± 0.8	17.3 ± 0.8	20.09 ± 0.9	14.85 ± 1.6
Porosity	1.13 ± 0.17	0.69 ± 0.04	0.14 ± 0.03	0.242 ± 0.009	0.102 ± 0.006	0.381 ± 0.015	0.046 ± 0.003

TABLE 4 Porosity and permeability statistics of typical wells in block B16 of the Xing'anling Formation.

Wells properties	B16 block									
	B16	B16	B16	B16	B110-2	B110-2	B106-2	B106-2	B106-2	B106-2
Permeability	12.81 ± 2.35	16.63 ± .58	25.64 ±2.73	15.63 ± 1.42	15.57 ± 1.61	11.55 ± 1.74	23.76 ± 2.23	23.95 ± 1.63	26.72 ± 3.42	25.38 ± 2.28
Porosity	0.005 ± 0.001	0.048 ± 0.002	24.2 ± 2.2	71.84 ± 5.16	0.047 ± 0.003	0.011 ± 0.002	44.03 ± 3.54	0.874 ± 0.048	3.29 ± 0.38	38.49 ± 2.94

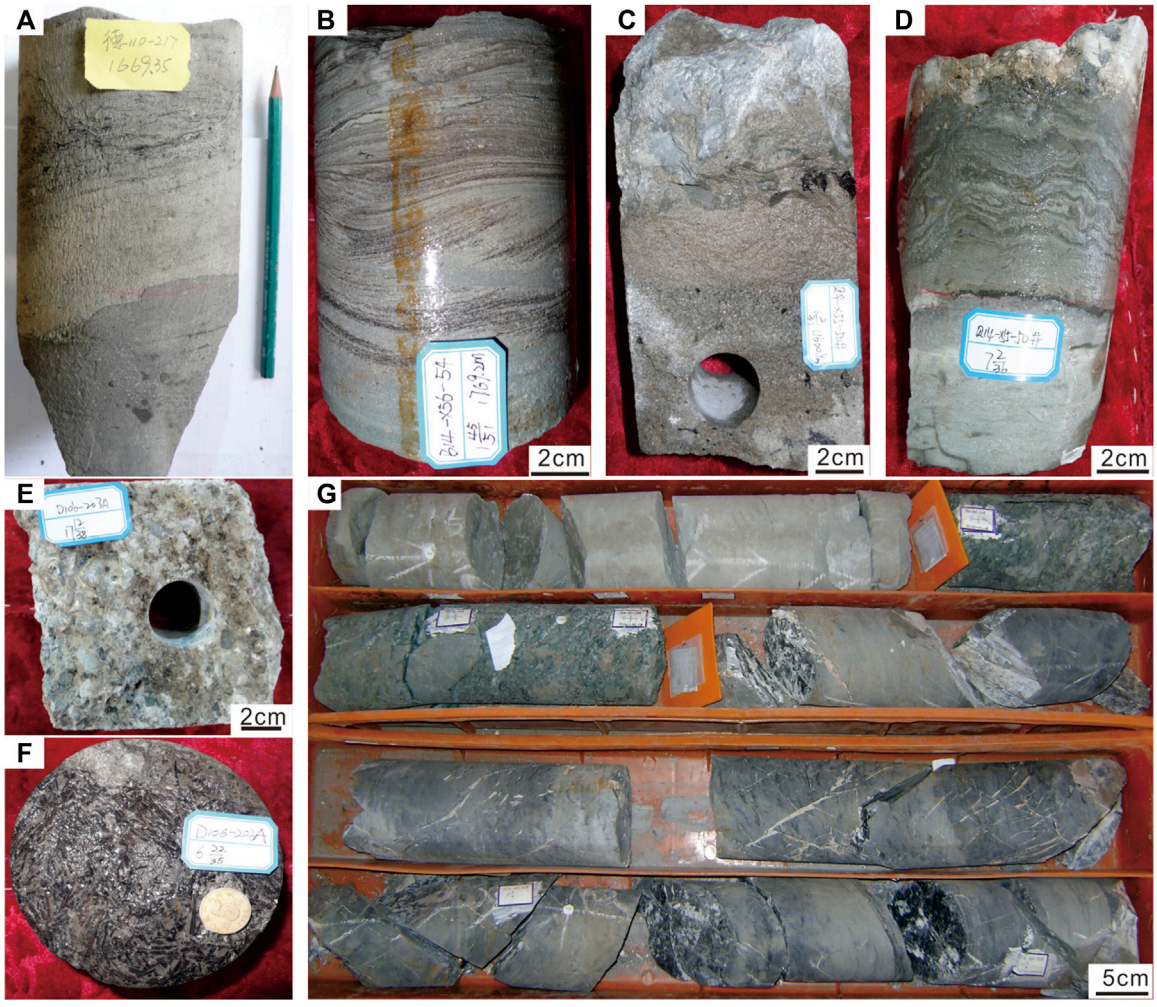

FIGURE 6
Core data showing the lithofacies and sedimentary features developed in the study area of the Xing'anling Formation. **(A)** D110-2. Depth, 1,669.35 m, abrupt contact between siltstone and mudstone. **(B)** B14-X5-1. Depth, 1769.2 m, wavy-cross bedding conglomerates. **(C)** B14-X6-1. Depth, 1,600.4 m, agitation structure. **(D)** B14-X6-1. Depth, 1645 m, crumple structure. **(E)** D106-1. Depth, 1,671.6 m, coarse sandstone. **(F)** D106-1. Depth 1,377.1 m, plant fossils. **(G)** B14-X6-1. Successive deposition of mudstone–siltstone–pebbly sandstone–siltstone conglomerate.

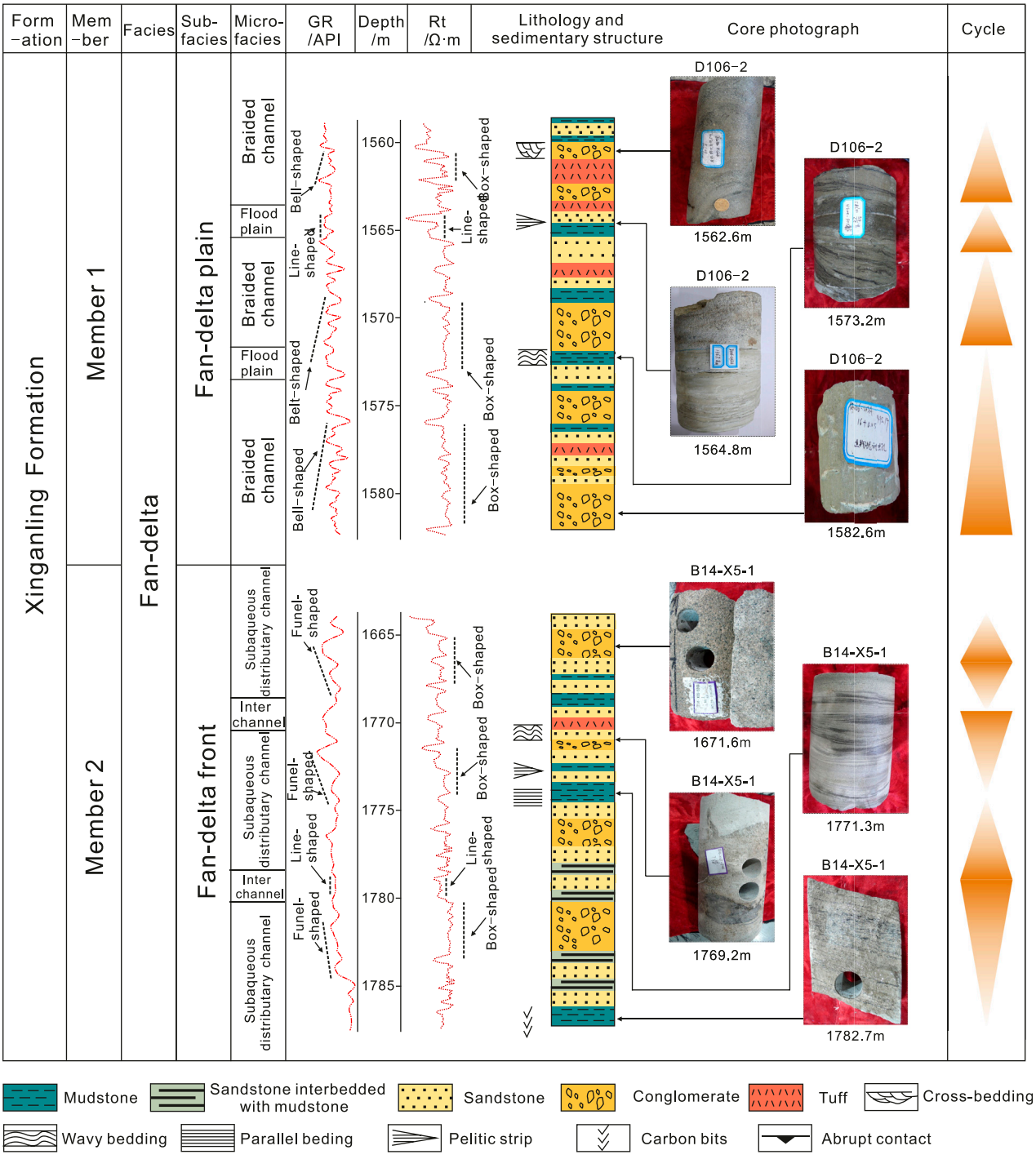

FIGURE 7
Core and well log characteristics of fan-delta plain deposits (D106-2) and fan-delta front deposits (well B14-X5-1) deposits. See details in the text (the site of the well is marked in Figure 1).

3.2.4 Facies types-fan-delta plain (evidence from typical wellbore core)

Core data (well D110-1 from block B16 over a depth interval of 1,669–1,681 m) showed that mudstone and muddy matrix in conglomerates or sandstones in the fan-delta plain were mainly gray in color (Figure 7). Massive, muddy-matrix-supported conglomerates, normal-grade, sandy matrix-supported conglomerates and massive, matrix-supported conglomerates only with basal erosional surface and massive, matrix-supported conglomerates with basal erosional surfaces and mud gravels were interpreted as braided channel fill deposits (Figures 6A–C–6C, 7) (Zakaria et al., 2013; Wei et al., 2017). The massive or horizontal bedding mudstones were gray in color and were interpreted as floodplain deposits (Figure 6) (Miall, 1977; Leila et al., 2022a; 2022b). Channel fill deposits always showed box-

shaped geometry on resistivity logs and funnel-shaped, bell-shaped or box-shaped geometry on gamma-ray logs (Figure 7). Floodplain deposits showed low-value, jagged geometry on gamma-ray logs and low-value line geometry on resistivity logs (Figure 7) (Morozov and Ma, 2009).

3.2.5 Facies types-fan-delta front (evidence from a typical wellbore core)

Core data (well B14-X5-4 from block B14 over a depth interval of 1,665–1782 m) showed that mudstones in the fan-delta front were mainly gray in color (Figure 7). Clast-supported granule conglomerates to conglomeratic sandstones, and mudstones are the dominant rock types (Figures 6A, B, D). Sedimentary structures generated by tractive currents are well developed in fan-delta front environments (Figures 6A, B, D) (Walker, 1978; Hein and Walker, 1982). Massive grain-supported conglomerates with basal erosional surfaces, normal graded grain-supported conglomerates, trough cross-bedding conglomerates and sandstones, parallel bedding sandstones, planar cross-bedding sandstones, and normal grading sandstones were interpreted as subaqueous distributary channel fill (Figure 6G). Reverse-grading sandstones, wavy cross-bedding sandstones, and sandstones with carbonized plant debris were interpreted as mouth bar deposits. The horizontal bedding mudstones were mainly gray in color and were interpreted as interchannel deposits. Subaqueous distributary channel fill deposits always showed high-value, bell-shaped or box-shaped geometry on resistivity logs and low-value, box-shaped or funnel-shaped geometry on gamma-ray logs (Figure 7). Interchannel deposits showed medium-value, jagged geometry on gamma-ray logs and low-value line geometry on resistivity logs (Figure 7) (Morozov and Ma, 2009).

3.3 Well correlations

In this study, the vertical sandstone-mudstone distribution characteristics of well correlations (Figures 8A, 9A) (AA' and BB' in Figure 1D) were clearly visible in the seismic sections (Figures 8B, 9B) after logging-constraint seismic inversion, which created conditions for identifying the sedimentary systems of well blocks B14 and B16 in the Sudeert fault zone (Figures 8C, 9C; the blocks are marked on Figure 1D).

Compared with mudstones, sandstones have a greater interval velocity (Eberhart-Phillips et al., 1989; Zhou et al., 2014) and can, therefore, be identified by their high acoustic impedance (Tarantola, 1984; Avseth et al., 2016). The lithological characteristics corresponding to different lacustrine sediments influence the seismic response and amplitude. In this study, sandstones with high acoustic impedance were characterized by a yellow color on impedance overlays; mudstones with lower acoustic impedance have dark colors (Figures 8B, 9B).

Based on two seismic profiles from the B14 and B16 well blocks (AA' and BB' in Figure 1D) and acoustic impedance data, together with borehole data, the distribution of the Xing'anling Formation across the study area has been reconstructed.

The fault-bound horsts in the seismic profiles are well blocks B16 and B14 (Figures 8C, 9C). A set of high-impedance reflectors appear at the bottom of the stratigraphy (M1–M4 in Figures 8B, 9B) and are interpreted as multi-stage sandstones (Figures 8C, 9C). These sandstones were deposited on top of the uplift of the Basement and their thicknesses increase close to the boundary faults (Figures 8C, 9C).

Some turbidite deposits characterized from core observations by matrix-supported, poorly sorted, and rounded sandy conglomerates occur locally in the footwall near the major faults (Figures 8, 9). The geophysical response characteristics of the turbidite sandstones are energy dispersive, with high acoustic impedance (Figures 8B, 9B).

The dark blue areas in the seismic sections (Figures 8B, 9B) correspond to sandy mudstones and mudstones interpreted to have been deposited in a lacustrine depositional system of deep water.

4 Sedimentary environments and distributions

Attribute slices allow the study of the distribution of sedimentary facies and sand bodies (Zeng et al., 2001; Zheng et al., 2016). Using the well data, the thickness maps of the sand bodies in Members 1 and 2 (Figures 10A, 11A) and the seismic attribute slices (Figures 10B, 11B), distribution of sedimentary facies was mapped for Members 1 and 2 of the Xing'anling Formation (Figures 10C, 11C). Three main types of depositional system were identified: fan-delta, lacustrine, and sub-lacustrine-fan (Table 5).

4.1 Fan deltas

Fan deltas are widely developed within the Xing'anling Formation (Figures 9C, 10C) and pro-delta, delta front, and delta plain facies were described (Nemec and Steel, 1988; Zakaria et al., 2013; Wei et al., 2016). In the study area, delta front deposits were dominant with distributary channels and mouth bars (Zakaria et al., 2013; Wei et al., 2016).

During the Xing'anling Formation deposition, the fan delta systems were mainly located in the central fault-bound high, including well blocks B28, B14, and B16, adjacent to the boundary faults (Figures 8–11). The plane graphs of the sedimentary facies indicate that large-scale fan delta fronts developed in block B16. The south of block B14 also contains delta front deposits, while several small, isolated delta lobes are present in block B28 (Figures 9C, 10C).

4.2 Lacustrine systems

The Sudeert fault zone shows two types of lacustrine deposits: shallow-lacustrine and deep-lacustrine (Figures 6–10). Deep-water lakes are characterized by dark-colored shale with high total organic carbon (TOC) content. The dark shale of the deep-lake facies is the main source rock for hydrocarbons in the Bell Depression (with TOC contents ranging from 0.16% to 4.73%, averaging 2.45%) (Xu et al., 2008b; Liu et al., 2010; Shan et al., 2010).

During the Xing'anling Formation deposition, the north part of blocks B14 and B16 formed the principal depocenter where deep-lacustrine sediments accumulated (Figures 10C, 11). Shallow-lacustrine deposits mainly developed in the south part of the Sudeert fault zone (Figures 10C, 11C).

4.3 Sub lacustrine fans

Sub lacustrine fans developed far from the lake shoreline (Normark and Dickson, 1976), e.g., in the downthrown side of

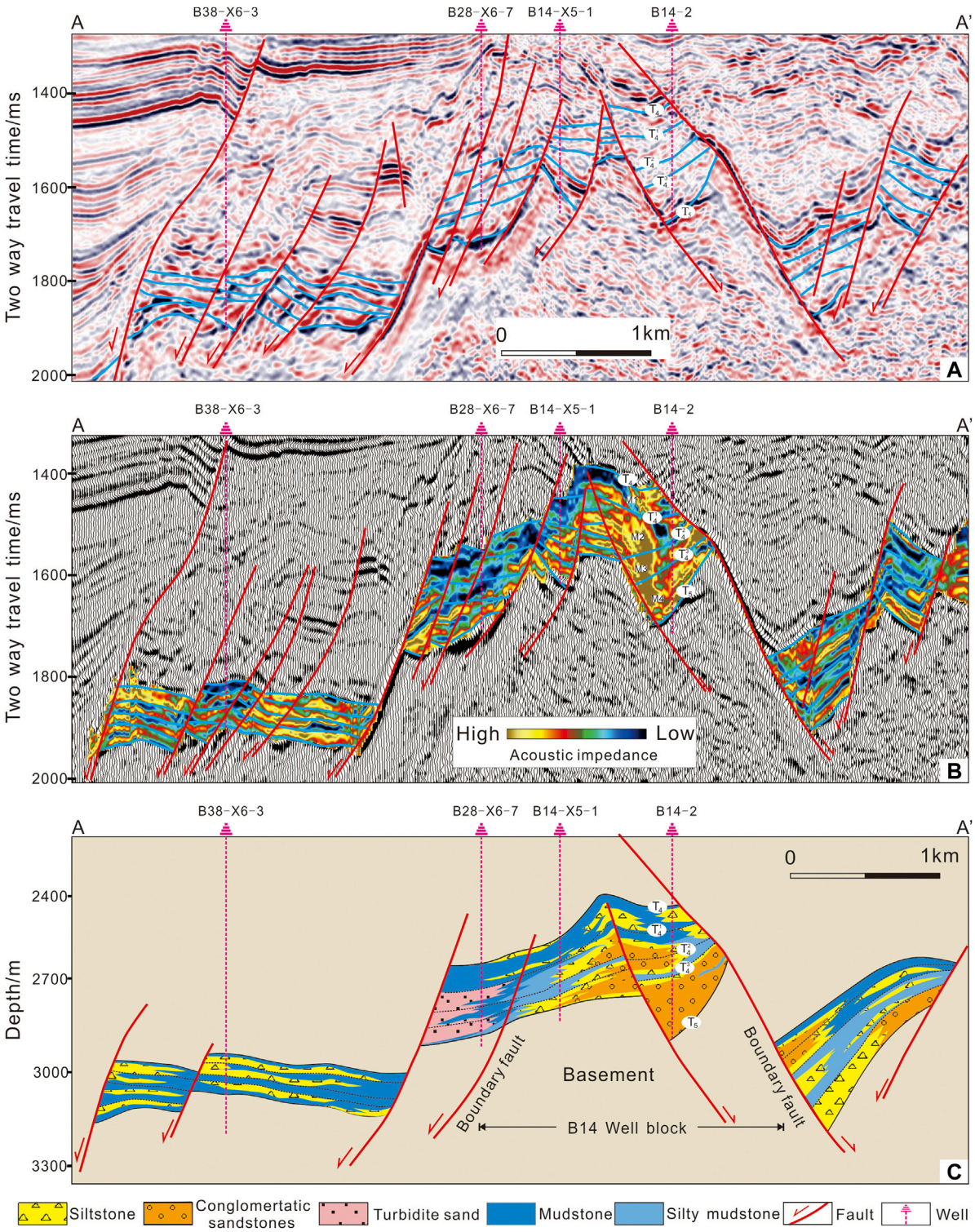

FIGURE 8
Profiles along a cross-section of wells B38-X6-3, B28-X6-7, B14-X5-1, and B14-2 in the Sudeert fault zone, Hailar Basin. **(A)** Seismic profile along cross-section AA' in Figure 1. **(B)** Acoustic impedance overlay. **(C)** Corresponding lithologic profile.

the major faults, e.g., in the north of block B14. The north part of block B14 includes a turbidite sand body surrounded by mudstones from the deep lacustrine system. A few examples of turbidite sand bodies surrounded by pro-delta mudstones are present in the western and northern parts of block B16 (Figures 10C, 11C).

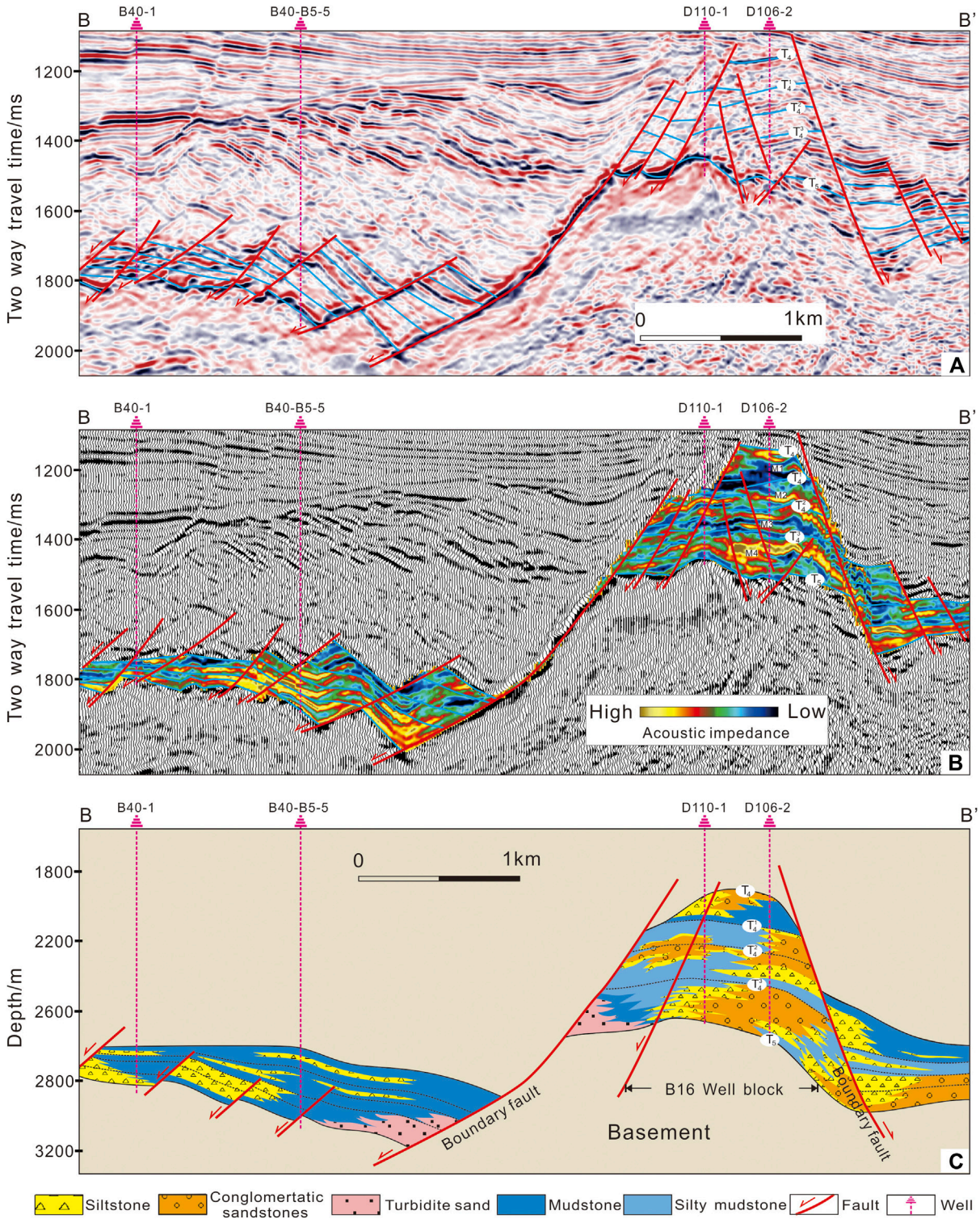

FIGURE 9
Profiles along a cross-section of wells B40-1, B40-B5-5, D110-1, and D106-2 in the Sudeert fault zone, Hailar Basin. **(A)** Seismic profile along a cross-section BB′ in Figure 1. **(B)** Acoustic impedance overlay. **(C)** Corresponding lithologic profile.

4.4 Regional sedimentary patterns

Three types of fan lobes were identified in blocks B28, B14, and B16: 1) isolated, 2) overlapping, and 3) superimposed lobes (Figure 12).

4.4.1 Isolated lobes

The western part of the study area, such as the area on the NW side of block B28 (Figures 1D, 12A), contains an isolated fan lobe system. Sandstone lobes here always exist in isolation (Figure 12A).

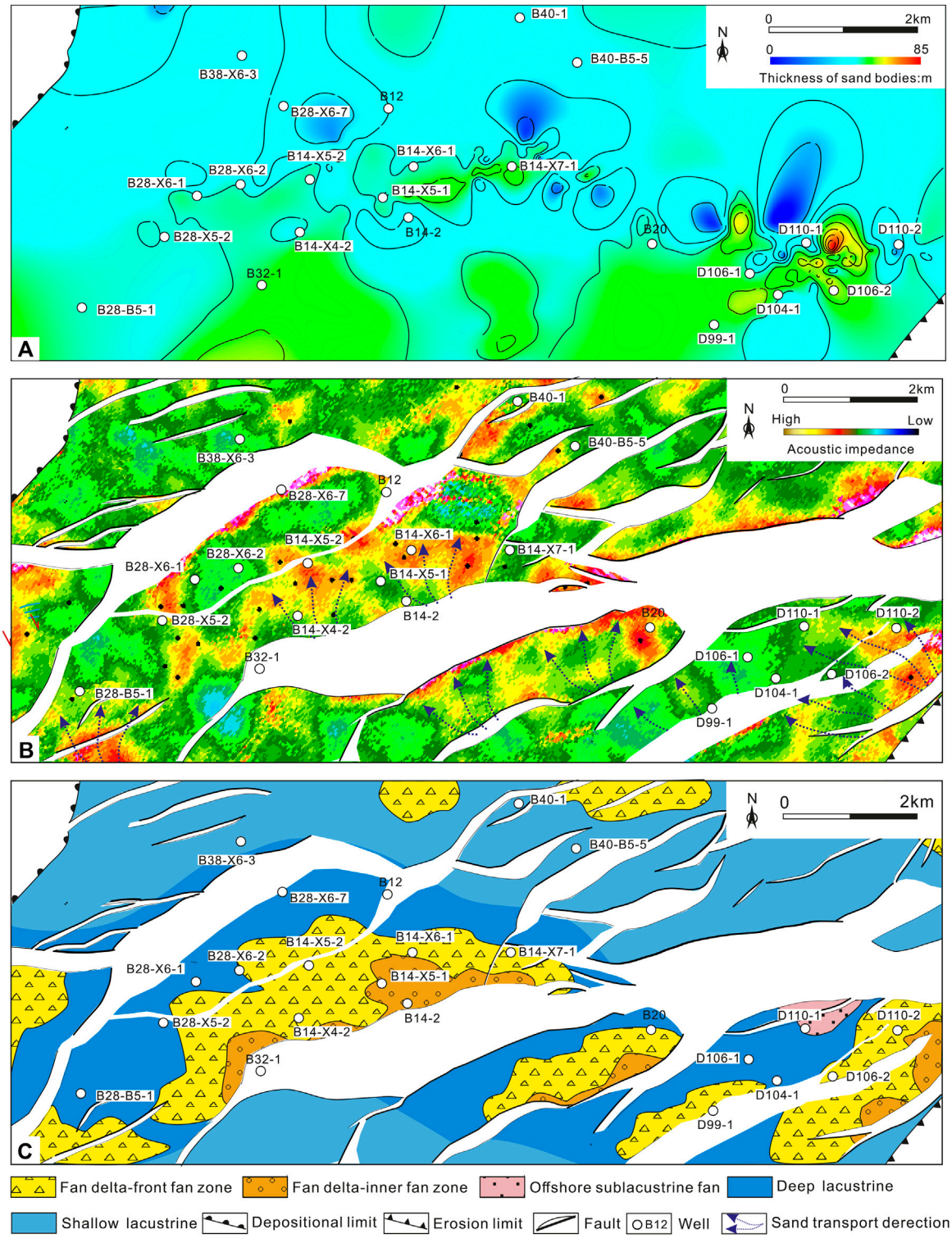

FIGURE 10
Map view distribution of the depositional systems in Member 1, including maps of the sandstone thickness **(A)**, absolute amplitude **(B)**, and interpreted depositional environment **(C)**.

Well section a-a' (Figure 12B) from the northern part of block B28 shows the sandstone distribution between wells. The sand bodies of well correlation are usually solitary (Figure 12C, well section of aa'). The lithofacies association from Member 1, Xing'anling Formation of block B28 includes mudstones, siltstones, and coarse sandstones from the top to bottom (Figure 12D) (such as

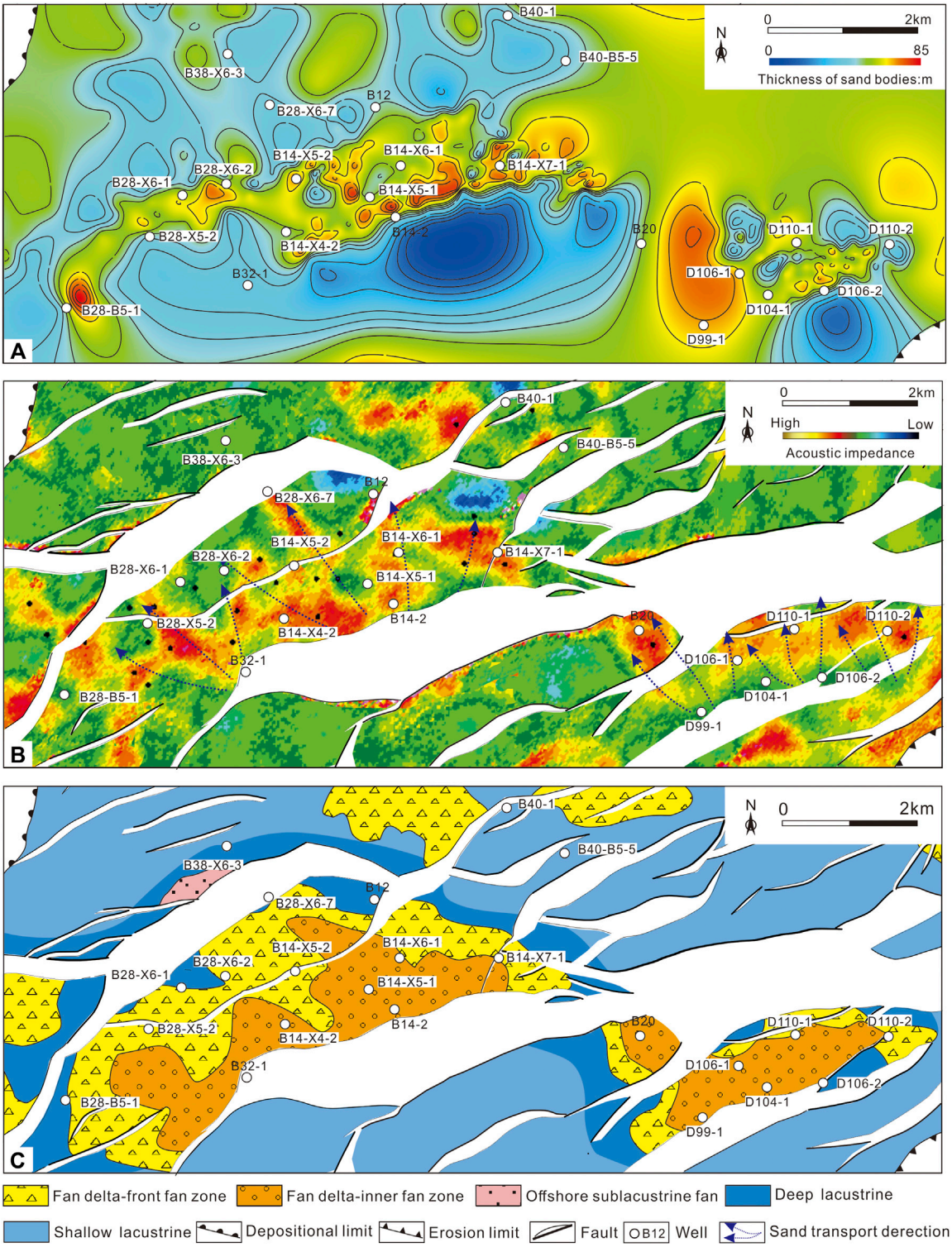

FIGURE 11
Map view distribution of the depositional systems in Member 2, including maps of the sandstone thickness **(A)**, absolute amplitude **(B)**, and interpreted depositional environment **(C)**.

the wells from B28-B5-1 to B28-X6-2). According to the lithological profile (Figure 12D) and sedimentary pattern (Figure 12E), the sedimentary facies assemblages of the pro-fan delta front and the fan delta front deposits vertically are the main sediment features of isolated lobes. In terms of plane, the lobes are shown as isolated, with no vertical or lateral contact (Figure 12E).

TABLE 5 Microfacies characteristics and types of Xing'anling Formation, Sudeert structural belt, Hailar Basin.

Depositional environment	Type		Channel	Lithology	Well logging characteristics	Sedimentary structure
	Sub-facies	Micro-facies				
Continental fan delta	Front margin of the fan delta	Submarine distributary channel	Yes	Medium to coarse sandstone with conglomerate	Medium to high box-shaped or tooth-shaped resistance	Flaser bedding
		Bank-attached bar sand of river channel margin	Yes	Medium-fine siltstone	Tooth-shaped resistance	Small-scale cross-stratification
		Estuary barrages	No	Medium-coarse sandstone	Funnel-shaped high-medium resistivity	Medium to small-scale cross-stratification
		Sheet-like sand	No	Siltstone, mudstone	Tooth-shaped resistance	Parallel bedding
Continental fan delta	Frontal fan delta	Turbidite sandstone	No	Fine siltstone	Tooth-shaped resistance	Bedding structure

4.4.2 Overlapping lobes

The central part of the study area, including part of block B14, contains overlapping fan lobes (Figures 1D, 12A) whose edges are in lateral contact (Figure 12A). Well section b-b' (Figure 12B) from Member 1, Xing'anling Formation of block B14 showed the distribution of sandstones between wells in this region (Figure 12B). The sand bodies of well correlation are usually overlapping (Figure 11C, well section of bb'). The lithofacies association from Member 2, Xing'anling Formation of block B14 often features multiple cycles from mudstone to coarse stone to siltstone (Figure 12D). Coarse sand bodies may be separated by mudstone. Parts of the siltstones are isolated (such as the upper part of the well B14-X4-2 stratigraphy); other sections of the coarse sand groups are continuous but thin (such as the lower part of the wells from B14-X5-1 to B14-X6-1). According to the lithological profile (Figure 12D) and sedimentary pattern (Figure 12E), the sedimentary facies assemblages of the fan delta front deposits and the fan delta plain deposit vertically are the main sediment features of the overlapping lobes. In terms of plane, the lobes overlap, with vertical or lateral stacking on the edges (Figure 12E).

4.4.3 Superimposed lobes

The eastern part of the study area, such as the NW area of block B16, contains a depositional system consisting of superimposed lobes (Figures 1D, 12A). Different stages and levels of fan delta lobes overlap vertically (Figure 12B).

Well section c-c' (Figure 12B) from block B16 shows the distribution of sandstones between wells (Figure 12C). The lithofacies association from Member 2 of block B16 of the Xing'anling Formation often consists of multiple positive cycles with relief at their bases (Figure 12D). Scoured bases and cross-bedding occur in these sand bodies (Figure 12D), with mudstone barriers in some sections within them. Conglomeratic sandstones were deposited above earlier, finer-grained sandstone. The sandstone units have good vertical communication. The crucial factor seems to have been the relatively narrow width of block B16 compared to the other regions under consideration; this led to the confinement of the sand input and the development of superimposed sand lobes. According to the lithological profile (Figure 12D) and sedimentary pattern (Figure 12E), the sedimentary facies assemblages of the fan delta plain deposit and the fan delta plain deposit vertically were the main sediment features of the superimposed lobes. In terms of plane, the lobes are superimposed, vertically or laterally stacked with each lobe body (Figure 12E).

5 Discussion

5.1 The geological evolution history of the fan delta sedimentation in the research area

Deposition of the Xing'anling Formation was divided into early syn-rift (Member 4), syn-rift (Members 4 and 3), and rift climax stages (Members 2 and 1) (Figures 5, 13A–C (Shan et al., 2010; Jia et al., 2014; Zhou et al., 2014). The planar distributions and vertical superposition relationships of the fan bodies in different blocks of the Sudeert fault zone were controlled by the ratio of accommodating space (A) to sediment input rate (S). The 3D structure of the top of the Sudeert fault zone shows a feature of "wide in the west and narrow in the east" with respect to the planar distribution of the fan bodies (Figure 12). Flattening the stratigraphy is a common technique in sedimentology to visualize the depositional environment. By flattening the top surface of Member 4 into two sections (with the same depth and scale) of well areas B28 (AA') and B16 (BB'), the accommodating space during the deposition of the Xing'anling Formation can be compared. The flattened surface is regarded as the lake level during the sedimentation period of the Xing'anling Formation, and the form of the bottom surface can be approximated as pre-sedimentary paleogeomorphic features. Although this method cannot precisely reconstruct the paleogeomorphic features of the Sudeert fault zone during the sedimentation period of the Xing'anling Formation, the size of the accommodating space in well areas B14 and B16 can be qualitatively compared under the assumption that the sediment input rate was constant across the study area. Figure 13 shows that compared with well area B14, the accommodating space in well area B16 has "narrow and deep" characteristics. In terms of sediment supply, the sand body thickness is an indicator of sediment input but does not necessarily reflect the sediment input rate. The sand body

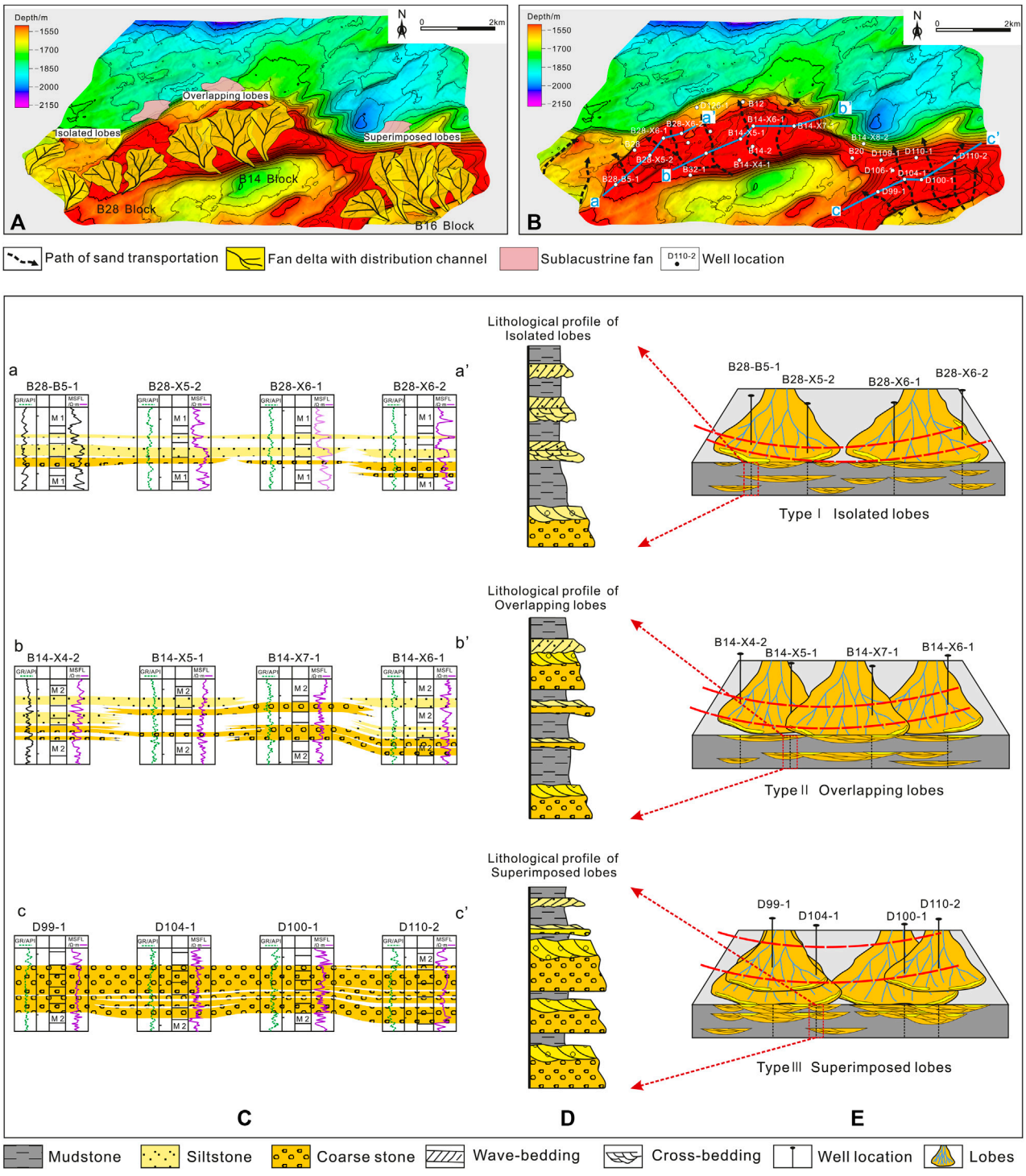

FIGURE 12
This figure shows the superposition relationships of fan delta lobes in different well blocks and the corresponding interwell correlation profiles. **(A)** The schematic diagram of the superposition relationships of fan delta lobes marked on the top structure map of the Member 2. **(B)** The transportation direction of sand bodies and the well locations of the interwell correlation profile used. **(C)** The vertical stacking relationships and lateral distribution patterns of sand bodies on the interwell correlation profiles under three different lobes relationships. **(D)** The schematic diagram of the three different lobe distribution characteristics and a vertical core section column chart. **(E)** Three types of fan-shaped lobes.

thickness in well area B16 was the largest, followed by well area B14, with well area B28 the smallest (Figure 6). This also indicated that the sediment input rate gradually decreased from west to east.

During the early syn-rift stage (Figure 13A), the deposition was mainly controlled by the inherited paleogeography, in which the sediments tend to accumulate in low-lying sags of the Basement (Zhou et al., 2014). Because of weak fault activity and shallow water

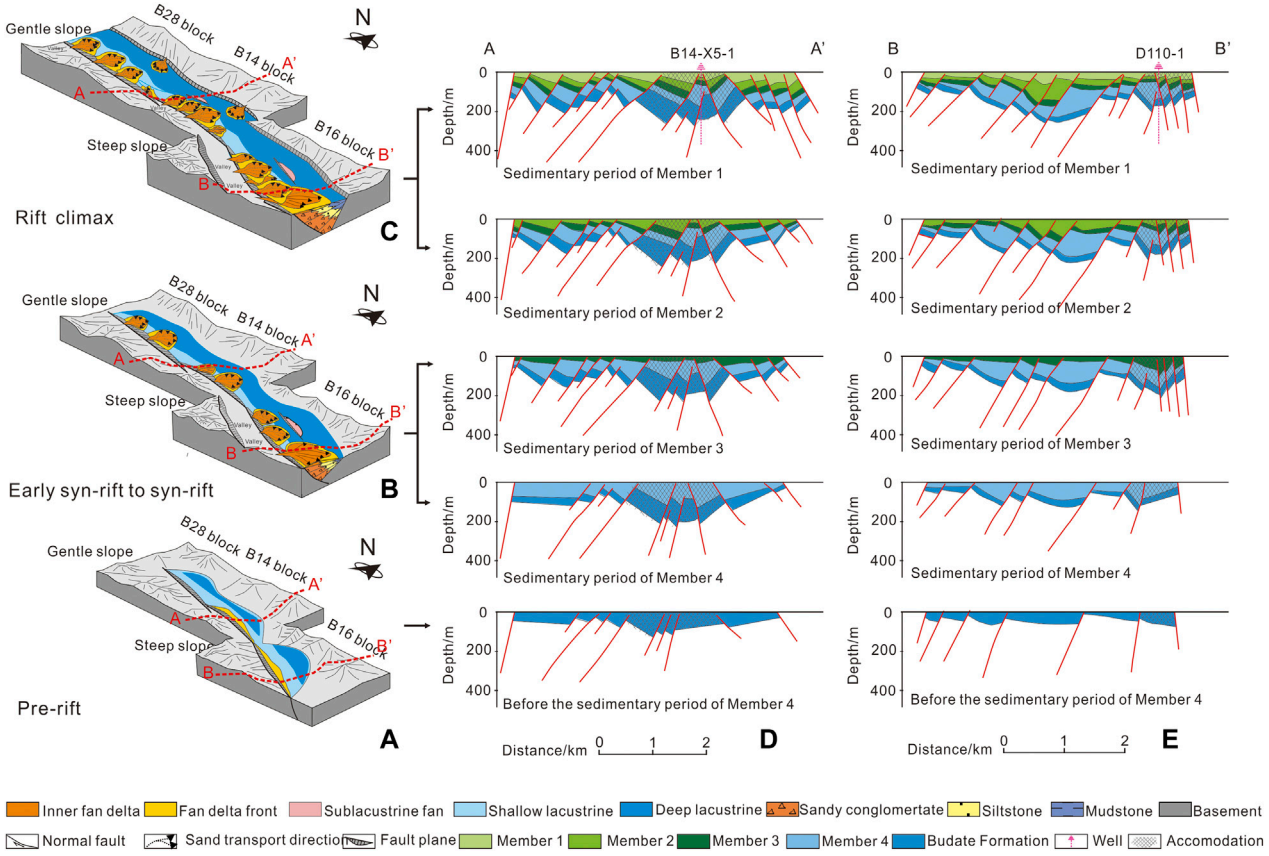

FIGURE 13
The figure shows a schematic diagram of the evolution model of the lobes of the fan delta from Xing'anling Formation in the Sudeert fault zone of Hailar Basin (scale not indicated). **(A)** Topography and fan distribution characteristics of the study area during the pre-rift stage. **(B)** Topography and fan distribution characteristics of the study area during the early syn-rift to syn-rift stage. **(C)** Topography and fan distribution characteristics of the study area during the rift climax stage. **(D)** The structural evolution section from well block B14 with labeled accommodation space for fan delta sedimentation. **(E)** The structural evolution section from well block B16 with labeled accommodation space for fan delta sedimentation.

depths, little deep water clastic deposition occurred in the study area (Figure 13A) (Liu et al., 2010) and shallow-water lacustrine deposition was dominant (Shan et al., 2010; Corella et al., 2016; Ballato, et al., 2017).

During the syn-rift stage (Figure 13B), oblique extension led to the formation of the Hailar Basin as a distinct feature (Ren et al., 2007) and was accompanied by a relative rise in lake level and increased accommodation (Figures 13D, E). Faults in the study area became more active (Shan et al., 2010; Fu et al., 2012), and sediments were largely derived from the southern uplift area (Figure 13B). Some isolated near-shore fan deltas developed in blocks B14, B28, and B16. Some source materials on the steeply dipping eastern shore were transported longer and formed subaqueous and sub-lacustrine fans near the eastern shore, especially in block B16, whose accommodation was the narrowest (Figure 13B).

From the late syn-rift to the rift climax stage, fault-driven subsidence caused a rapid relative rise of lake level (Wang et al., 2007; Yu et al., 2013) as a result of which the accommodation increased and three depo-centers of different sizes developed. According to the chart of sand body deposition thickness (Figures 10A, 11A), it can be intuitively found that the sand bodies of block B16 is the thickest, followed by block B14 and B28 in that order. This also indicates that the sand bodies supply was gradually decreasing from west to east during the sedimentary periods of Members 2 and 1. With an abundant supply of source, many of the near-shore fan deltas developed in blocks B14, B28, and B16 (Figure 13C). As shown in Figures 13D, E, the accommodation of the block B16 area was "narrower and deeper" than that of block B14; therefore, superimposed sand bodies formed more readily (Figure 13C) (Einaby and Ei-aai, 2016; Wang, et al., 2016; Deaf et al., 2020).

The balance between the accommodation generated by tectonic subsidence and lake-level fluctuations versus sediment input may have been responsible for the formation of the different lacustrine facies types in the study area (Lin et al., 2008). Isolated lobes would have developed in response to scarce sand input and slowly increasing accommodation. The sand input was insufficient to form multiphase fan delta lobes and only a few isolated lobes were formed in the western part of the study area, e.g., in block B28. The formation of contact lobes

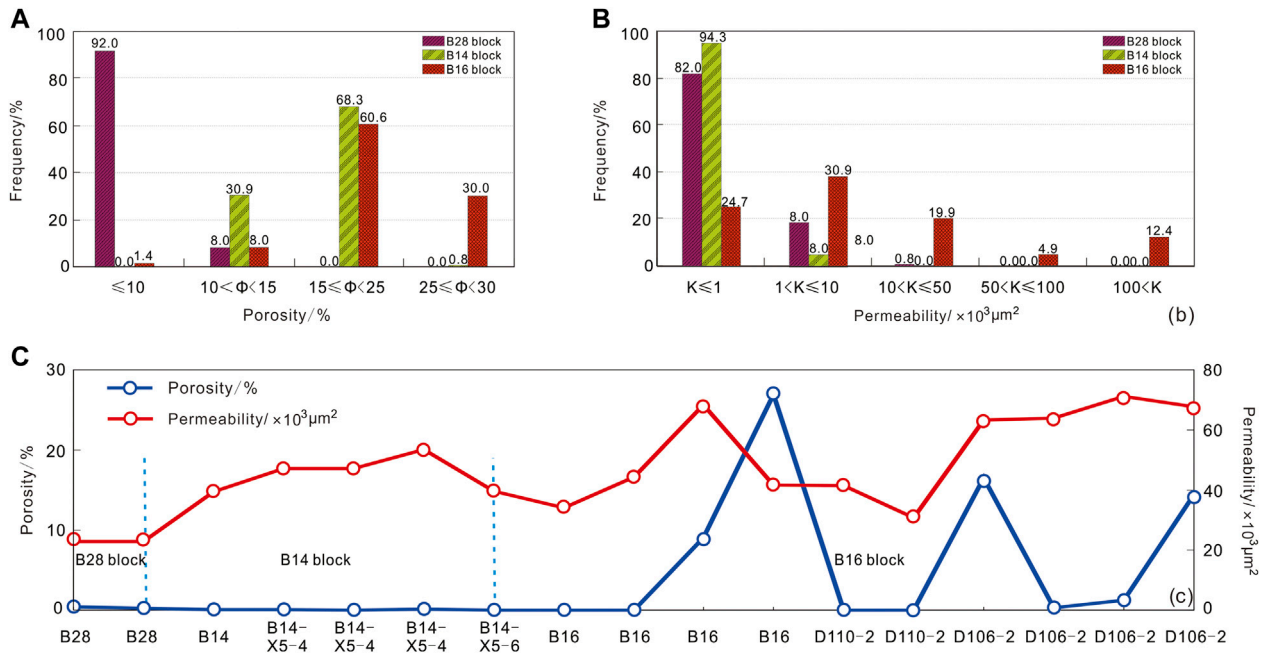

FIGURE 14
Bar graph of the porosity statistics for blocks B28, B14, and B16 of the Xing'anling Formation **(A)**. Bar graph of the permeability statistics for blocks B28, B14, and B16 of the Xing'anling Formation **(B)**. Line chart of porosity and permeability in blocks B28, B14, and B16 **(C)**.

would have been favored by a greater sediment supply and by steadily increasing accommodation across a wider area (Su et al., 2011). When a deltaic channel migrated laterally, it formed a new lobe, which stayed connected to the initial lobe. Block B14 typifies this type of behavior.

Superimposed lobes were formed when adequate sediment input was combined with steadily increasing accommodation in a restricted area. Fan lobes formed during the early stages did not completely occupy the accommodation (Figures 13D, E). Accommodation developed in a narrow area; thus, the channels migrated laterally but formed new lobes, which stayed connected to the former lobes. Late-stage lobes were vertically superimposed on earlier lobes. Block B16 typifies this type of deposition.

5.2 Petroleum geology significance

The reservoir in the Sudeert oil field is highly heterogeneous and generally poor in physical properties (Wang, 2019). The physical properties of the reservoir are obviously controlled by the regional sedimentary patterns and the combination of sand bodies, consistent with the overlapping rule of sand bodies in each block (Figures 12, 13).

Block B16 showed the best permeability because the lobe sand bodies in this area are superimposed and have good porosity (Figure 14). Meanwhile, the intersections between different fan bodies strengthen the connectivity between different fan sand bodies, thus increasing the reservoir permeability (Figure 14C). The sand bodies in the block B14 lobes have developed better vertical superimposed relationships and high porosity, but in terms of horizontal sand bodies connection, a contact relationship (overlapping) between different lobes only exists on the edge of the lobes. Although the sand bodies inside the fan lobes have good connectivity, the lack of horizontal connection between multiple fan bodies leads to poor permeability (Figure 14C). However, block B28 is the poorest, with fewer fan lobes formed, most of which are solitary fans (Figures 12, 13), leading to poor reservoir physical properties (Figure 14C).

Member 2 in the Sudeert oil field has the highest oil production, mainly due to its high-quality reservoir (Figure 15). The fan body lobes are large, and the main channel is vertically intersected and vertically overlapped. Meanwhile, the shape of the lobes inside the same fan determines the movement of oil and water in this area. High-production wells mainly concentrate in solitary lobes where sand bodies are well developed and have strong connectivity. Excluding the artificial fractures in parts of the well area, the high production occurs mainly due to the formation of solitary lobes during the same period and from the same sources, resulting in little physical property differences in the lobes, which are conducive to the overall movement of oil and water.

In the sedimentation process of oil and gas reservoirs, a "narrow and deep" paleogeomorphic environment, such as the B16 block in the Suderte oil field, is most conducive to the spatial superposition of fan-shaped sedimentary systems, thus forming a favorable development pattern for oil and gas reservoirs. These findings are of inspiring significance to the general public, as they reveal the factors that control the production capacity of oil and gas in basins. A similar example can be found in the Alberta Basin in Canada, where the Devonian and Cretaceous formations contain abundant oil and gas resources (Gibbs and Rakhit, 2019), which are clearly

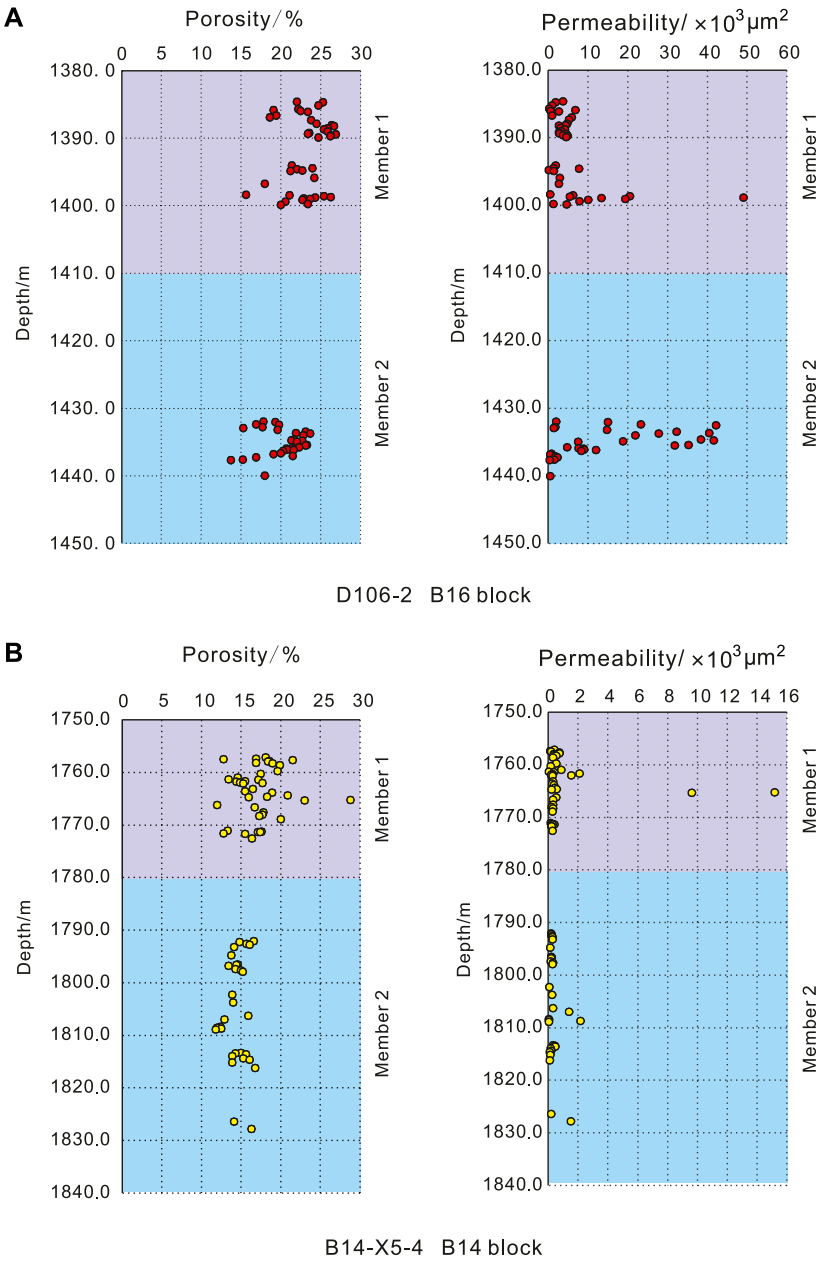

FIGURE 15
Distribution characteristics of porosity and permeability at different depths in the Member 1 and 2 groups of two typical wells, D106-2 **(A)** and B14-X5-4 **(B)**, in the blocks B16 and B14.

controlled by the sedimentary characteristics of the formations (Posamentier et al., 1992). Due to the large-scale thrusting of the Rocky Mountains towards the basin since the Cenozoic, a large-scale thrusting structural style has formed on the western margin of the Alberta Basin (Michael and Bachu, 2001), similar to the B16 well area in the present study. The "narrow and small" triangular belt structure formed by the reverse thrusting on the western edge of the Alberta Basin is the most favorable area for the accumulation of oil and gas reservoirs (Bennett and Jiang, 2021), as this type of sedimentary space is more conducive to the interlayering of clastic sediments in the reservoir, thus forming high-quality reservoirs.

6 Conclusion

This study focused on a lacustrine fan system in the Lower Cretaceous Xing'anling Formation in the Beier Sag, Hailar Basin, NE China. Three main depositional facies were identified: fan delta, lacustrine system, and sub-lacustrine fan. Deposition was primarily controlled by extensional tectonics, but the extent to which climatic variations affected stratigraphy at different spatial scales remains unclear.

The overlapping fan lobes in different well blocks developed in response to varying levels of sediment input and accommodation,

resulting in different sand body depositional patterns. The results showed that overlapping lobes with high connectivity and overall sand volume were the most favorable for forming high-quality reservoir units for hydrocarbons.

In addition to sedimentary processes, tectonic activity can also contribute to the formation of oil and gas reservoirs. Faults and folds can trap hydrocarbons and create areas of high pressure that facilitate oil and gas migration and accumulation. Over time, changes in the basin geology can also lead to changes in the location and quality of oil and gas reservoirs. A comprehensive understanding of the sedimentary and tectonic processes that contribute to reservoir formation is critical for the exploration and production of hydrocarbon resources.

Overall, the results of this study shed light on the complex factors that control the formation of reservoirs in lacustrine fan systems and have implications for the oil and gas industry, such as informing exploration and production strategies and identifying new areas for resource development.

Data availability statement

The original contributions presented in the study are included in the article/Supplementary Material. Further inquiries can be directed to the corresponding author.

Author contributions

XC: conceptualization, methodology, software, investigation, formal analysis, and writing—original draft; JL: conceptualization; HJ: data analysis and investigation; HY: data analysis and writing; QQ: data analysis and constructive discussions.

Funding

This work is supported by Fund of National Key Laboratory of Science and Technology on Remote Sensing Information and Imagery Analysis, Beijing Research Institute of Uranium Geology (Grant No. 6142A01210101) and (No. 6142A01180401) and the National Basic Research Program of China (No. 41602333).

Acknowledgments

The authors would like to express their gratitude to Mark Allen from the Department of Earth Sciences, Durham University, for his assistance with the article's ideas, structure, and discussion section. They also thank Stuart Jones from the Department of Earth Sciences, Durham University, for his suggestions and assistance with the study of sedimentary environments. The authors would like to thank the personnel of CNPC Hailar Exploration and Development Administration and Daqing Oilfield Company for their assistance with core description and data collection. Lastly, they would like to thank Liu Zhonglan, Zhang Hongwei, Xu Li, and Wang Hui from the School of Earth and Space Sciences, Peking University, for their help and support during the research process.

Conflict of interest

XC was employed by CNNC, HJ was employed by Daqing Oilfield Company, HY was employed by CNPC Institute of Liaohe Oilfield, and QQ was employed by Shuguang Oil Production Plant of Liaohe Oilfield Company.

The remaining authors declare that the research was conducted in the absence of any commercial or financial relationships that could be construed as a potential conflict of interest.

Publisher's note

References

Allen, M. B., Macdonald, D. I. M., Xun, Z., Vincent, S. J., and Brouet-Menzies, C. (1997). Early Cenozoic two-phase extension and late Cenozoic thermal subsidence and inversion of the Bohai Basin, northern China. *Mar. Petroleum Geol.* 14, 951–972. doi:10.1016/s0264-8172(97)00027-5

Asim, S., Ahmad, S., Zhu, P., Naseer, M. T., and Butt, M. (2016) Spectral decomposition application for analyzing the structure and the reservoir potential: A case study of penobscot, nova scotia offshore, Canada. *Arabian J. Geosciences*, 9, 1–20. doi:10.1007/s12517-015-2168-x

Avseth, P., Janke, A., and Horn, F. (2016). AVO inversion in exploration—key learnings from a Norwegian sea prospect. *Lead. Edge* 35, 405–414. doi:10.1190/tle35050405.1

Ballato, P., Cifelli, F., Heidarzaseg, G., Ghassemi, M. R., Wickert, A. D., Hassanzadeh, J., et al. (2017). Tectono-sedimentary evolution of the northern Iranian Plateau: Insights from middle–late Miocene foreland-basin deposits. *Basin Res.* 29, 417–446. doi:10.1111/bre.12180

Bennett, B., and Jiang, C. (2021). Oil-source and oil-oil correlations and the origin of the heavy oil and bitumen accumulations in northern Alberta, Canada. *Org. Geochem.* 153, 104199. doi:10.1016/j.orggeochem.2021.104199

Chen, J., Wu, H., Zhu, D., Lin, C., and Yu, D. (2007) Tectonic evolution of the Hailar basin and its potentials of oil-gas exploration. *Chin. J. Geol.*, 42, 147–159. (in Chinese with English abstract).

Chopra, S., and Marfurt, K. (2006). Seismic Attributes–a promising aid for geologic prediction. *CSEG Rec.* 31, 110–120.

Corella, J., Loizeau, J.-L., Kremer, K., Hilbe, M., Gerard, J., Le Dantec, N., et al. (2016). The role of mass-transport deposits and turbidites in shaping modern lacustrine deepwater channels. *Mar. Petroleum Geol.* 77, 515–525. doi:10.1016/j.marpetgeo.2016.07.004

Cui, X., Li, J., Yang, S., Li, W., and Ma, L. (2016) Hydrocarbon accumulation in rifted basin tectonic units: A case study of huoduomoer tectonic zone in the hailaer basin. *Petroleum Geol. Exp.*, 38, 40–47. (in Chinese with English abstract).

Deaf, A. S., Tahoun, S. S., Gentzis, T., Carvajal-Ortiz, H., Harding, I. C., Marshall, J. E., et al. (2020). Organic geochemical, palynofacies, and petrographic analyses examining the hydrocarbon potential of the Kharita Formation (Albian) in the Matruh Basin, northwestern Egypt. *Mar. Petroleum Geol.* 112, 104087. doi:10.1016/j.marpetgeo.2019.104087

Dou, L., and Chang, L. (2003). Fault linkage patterns and their control on the formation of the petroleum systems of the Erlian Basin, Eastern China. *Mar. Petroleum Geol.* 20, 1213–1224. doi:10.1016/j.marpetgeo.2003.07.002

Eberhart-Phillips, D., Han, D.-H., and Zoback, M. D. (1989). Empirical relationships among seismic velocity, effective pressure, porosity, and clay content in sandstone. *Geophysics* 54, 82–89. doi:10.1190/1.1442580

Einaby, A. I. A., and Ei-aai, M. A. (2016). Tectono-sedimentary evolution of active extensional basins controlling the deposition of the Middle Miocene Kareem Formation, southwestern Gulf of Suez, Egypt. *Arabian J. Geosciences* 9, 1–14.

Feng, Y., Jiang, S., Hu, S., Li, S., Lin, C., and Xie, X. (2016). Sequence stratigraphy and importance of syndepositional structural slope-break for architecture of Paleogene syn-rift lacustrine strata, Bohai Bay Basin, E. China. *Mar. Petroleum Geol.* 69, 183–204. doi:10.1016/j.marpetgeo.2015.10.013

Feng, Z. Q., Jia, C. Z., Xie, X. N., Shun, Z., Feng, Z., and Cross, T. A. (2010). Tectonostratigraphic units and stratigraphic sequences of the non-marine Songliao basin, northeast China. *Basin Res.* 22, 79–95. doi:10.1111/j.1365-2117.2009.00445.x

Feng, Z., Sun, G., Meng, Q., and Feng, Z. (2011). Beizhong Sub-Depression in the Hailaer Basin:A successful case for oil exploration in small residual superimposed rift basins. *Acta Geol. Sin.* 32, 551–563. (in Chinese with English abstract).

Folk, R. L. (1954). The distinction between grain size and mineral composition in sedimentary-rock nomenclature. *J. Geol.* 62, 344–359. doi:10.1086/626171

Fu, X., Jing, D., and Lu, Y. (2012). Fault structural characteristics of Wuerxun-Beier Depression in the Hailar basin and their reservoir-controlling mechanism. *Acta Geol. Sin.* 86, 877–889. (in Chinese with English abstract).

Gibbs, A., and Rakhit, K. (2019). "Hydrodynamics, geothermics and spatial variations in hydrocarbon fluid distribution within the Montney Formation, Alberta and British Columbia, Canada," in *SPE annual technical conference and exhibition* (OnePetro).

Hein, F. J., and Walker, R. G. (1982). The cambro-ordovician cap enragé formation, queébec, Canada: Conglomeratic deposits of a braided submarine channel with terraces. *Sedimentology* 29, 309–352. doi:10.1111/j.1365-3091.1982.tb01798.x

Jia, J., Liu, Z., Miao, C., Fang, S., Zhou, R., Meng, Q. A., et al. (2014). Depositional model and evolution for a deep-water sublacustrine fan system from the syn-rift lower cretaceous Nantun Formation of the tanan depression (tamtsag basin, Mongolia). *Mar. Petroleum Geol.* 57, 264–282. doi:10.1016/j.marpetgeo.2014.05.022

Kang, D., Pang, X., and Zhang, Y. (2008). Reservoir properties of Suderte buried hill and main controlling factors, Beir Depression, NE China. *Petroleum Explor. Dev.* 35, 188–194. (in Chinese with English abstract). doi:10.1016/s1876-3804(08)60026-9

Kang, L., Sun, Y., Liu, B., Hou, Z., and Sun, R. (2013). Controlling effect of fault system on formation evolution and reservoir formation of buried hill in middle fault depression belt in Hailer - tamtsag Basin. *J. Central South Univ. Sci. Technol.* 44, 2417–2427. (in Chinese with English abstract).

Leila, M., El Sharawy, M., Bakr, A., and Mohamed, A. K. (2022b). Controls of facies distribution on reservoir quality in the Messinian incised-valley fill Abu Madi Formation in Salma delta gas field, northeastern onshore Nile Delta, Egypt. *J. Nat. Gas Sci. Eng.* 97, 104360. doi:10.1016/j.jngse.2021.104360

Leila, M., Yasser, A., El Bastawesy, M., and El Mahmoudi, A. (2022a). Seismic stratigraphy, sedimentary facies analysis and reservoir characteristics of the Middle Jurassic syn-rift sediments in Salam Oil Field, north Western Desert, Egypt. *Mar. Petroleum Geol.* 136, 105466. doi:10.1016/j.marpetgeo.2021.105466

Li, C. B. (2021). Petroleum exploration history and enlightenment in Hailar Basin. *Xinjiang Pet. Geol.* 42 (3), 374. (in Chinese with English abstract).

Li, Z., Yu, P., Shao, B., Bao, C., Ma, J., Zhu, X., et al. (2015). Response analysis of sedimentary filling evolution and tectonic activity incomplicated faulted basin: An example of middle rift belt in hailar-tamtsag basin. *J. China Univ. Min. Tecnology* 44, 853–858. (in Chinese with English abstract). doi:10.1002/mc.22156

Lin, C., Eriksson, K., Sitian, L., Yongxian, W., Jianye, R., and Yanmei, Z. (2001). Sequence architecture, depositional systems, and controls on development of lacustrine basin fills in part of the Erlian basin, northeast China. *AAPG Bull.* 85, 2017–2043.

Lin, C., Liang, C., Ren, L., and Zhu, Y. (2008). Sedimentary facies and ralation to degree of fracture developemt of clastic buried hills. *J. China Univ. Petroleum* 32, 1–6. (in Chinese with English abstract).

Lin, C. S., Zheng, H. R., Ren, J. Y., Liu, J. Y., and Qiu, Y. G. (2004). The control of syn-depositional faulting on the Eogene sedimentary basin fills of the Dongying and Zhanhua sags, Bohai Bay Basin. *Sci. China Ser. D Earth Scineces-English Ed.* 47, 769–782. doi:10.1360/03yd0203

Liu, Q., Lu, S., Li, J., Chen, X., and Hu, S. (2010). Sequence stratigraphy and sedimentary system analysis of Nantun group in huhehu depression in Hailar Basin. *Acta Geol. Sin.* 28, 227–234. (in Chinese with English abstract).

Liu, S., Gao, G., Zhu, D., Wu, G., Wang, J., Zhang, G., et al. (2015). Early cretaceous fracturing and basin evolution of the south buir sag of the tamtsag Basin in Mongolia. *Geotect. Metallogenia* 39, 780–794. (in Chinese with English abstract).

Miall, A. D. (1977). A review of the braided-river depositional environment. *Earth-Science Rev.* 13 (1), 1–62. doi:10.1016/0012-8252(77)90055-1

Michael, K., and Bachu, S. (2001). Fluids and pressure distributions in the foreland-basin succession in the west-central part of the Alberta Basin, Canada: Evidence for permeability barriers and hydrocarbon generation and migration. *AAPG Bull.* 85 (7), 1231–1252.

Morozov, I. B., and Ma, J. (2009). Accurate poststack acoustic-impedance inversion by well-log calibration. *Geophysics* 74 (5), R59–R67. doi:10.1190/1.3170687

Nemec, W., and Steel, R. (1988). *Fan deltas: Sedimentology and tectonic settings*, 3–13.What is a fan delta and how do we recognize it

Normark, W. R., and Dickson, F. H. (1976). Sublacustrine fan morphology in lake superior. *AAPG Bull.* 60, 1021–1036.

Posamentier, H. W., Allen, G. P., and James, D. P. (1992). High resolution sequence stratigraphy; the east coulee delta, Alberta. *J. Sediment. Res.* 62 (2), 310–317.

Ren, J., Tamaki, K., Li, S., and Junxia, Z. (2002). Late Mesozoic and Cenozoic rifting and its dynamic setting in Eastern China and adjacent areas. *Tectonophysics* 344, 175–205. doi:10.1016/s0040-1951(01)00271-2

Ryder, R. T., Fouch, T. D., and Elison, J. H. (1976). Early tertiary sedimentation in the Western uinta basin, Utah. *Geol. Soc. Am. Bull.* 87, 496–512. doi:10.1130/0016-7606(1976)87<496:etsitw>2.0.co;2

Shan, J., Wang, F., Sun, H., Sun, J., and Meng, Q. (2010). Depositional tectonic sequences evolvement of sedimentary system by syngenesis fracture integrated mode: An example from tabel depression in monglia. *Geol. Rev.* 6, 426–439. (in Chinese with English abstract).

Su, J., Zhu, W., Wei, J., Xu, L., Yang, Y., Wang, Z., et al. (2011). Fault growth and linkage: Implications for tectonosedimentary evolution in the chezhen basin of Bohai bay, eastern China. *AAPG Bull.* 95, 1–26. doi:10.1306/06301009207

Sun, Y., Yu-ping, H., Zhi-peng, F., Xiao-fei, F., and Zhe, L. (2011). Fault systems and its control on hydrocarbon migration and accumulation in Beier Sag, Hailar Basin. *Geol. Rev.* 57, 89–90. (in Chinese with English abstract).

Tarantola, A. (1984). Inversion of seismic reflection data in the acoustic approximation. *Geophysics* 49, 1259–1266. doi:10.1190/1.1441754

Torres Verdin, C., Victoria, M., Merletti, G., and Pendrel, J. (1999). Trace-based and geostatistical inversion of 3-D seismic data for thin-sand delineation: An application in San Jorge Basin, Argentina. *Lead. Edge* 18, 1070–1077. doi:10.1190/1.1438434

Traynor, J., and Sladen, C. (1995). Tectonic and stratigraphic evolution of the Mongolian People's Republic and its influence on hydrocarbon geology and potential. *Mar. Petroleum Geol.* 12, 35–52. doi:10.1016/0264-8172(95)90386-x

Valencia, M. J. (1989). Northeast Asia: Petroleum potential, jurisdictional claims, and international relations. *Ocean Dev. Int. Law* 20, 35–61. doi:10.1080/00908328909545879

Walker, R. G. (1978). Deep-water sandstone facies and ancient submarine fans: Models for exploration for stratigraphic traps. *AAPG Bull.* 62, 932–966.

Wang, J., Fan, T., Wang, H., Liu, Z., Li, Y., and Hu, X. (2012). Reservoir heterogeneity characteristics in the framework of multi grade base level cycle of the oil layers of Tongbomiao and Nantun Formations in the Sudeerte Oil Field. *Geosci. Front.* 19, 10–22. (in Chinese with English abstract).

Wang, S., Wang, P., Jin, Z., and Jiang, L. (2007). Geological features and genetic interpretation of sudeerte buried-hill traps of hailaer basin, E China. *J. Jilin Univ. (Earth Sci. Ed.* 37, 79–85. (in Chinese with English abstract).

Wang, X., Jiang, Z., Yuan, S., Wang, H., and Sun, K. (2016). Metabolically obese individuals of normal weight have a high risk of 25-hydroxyvitamin D deficiency. *Geol. J. China Univ.* 22, 360–367. (in Chinese with English abstract). doi:10.1016/j.amjms.2016.06.017

Wang, Y, H. (2019). Analysis and countermeasure on the exploration situation of Daqing Oilfield. *Petroleum Geol. Oilfield Dev. Daqing* 38, 23–33.

Wei, W., Zhu, X., Tan, M., Wu, C., Guo, D., Su, H., et al. (2017). Facies controls on the distribution of diagenetic alterations in fan delta deposits: A case study from the lower cretaceous sandstone, chagan sag, inner Mongolia, China. *Geol. J.* 52, 539–558. doi:10.1002/gj.2788

Wu, H., Li, Z., Feng, Z., and Zhu, D. (2006). Analysis on structural features and reservoir-forming process of Wuerxun and Beier sags in Hailar Basin. *Acta Pet. Sin.* 27, 1–6. (in Chinese with English abstract).

Xu, Z., Yao, J., Wang, X., and Zhang, D. (2008a). Reservoir sedimentary characteristics and heterogeneity of block bei 16, xing'anling group in sudeerte oil field. *J. Jilin Univ. (Earth Sci. Ed.* 38, 926–932. (in Chinese with English abstract).

Xu, Z., Yao, J., Wang, X., Zhang, D., and Zhang, W. (2008b). Sedimentary microfacies and gas/oil distribution in I oil Formation in xing'anling group, sudeerte oilfied. *Nat. Gas. Geosci.* 19, 680–684. (in Chinese with English abstract).

Yi, J., Wang, P., Tang, H., Zhao, R., Yao, R., Hao, G., et al. (2015). Geological property, geological connotation and reservoir significance of volcano stratigraphic boundary: A case study of the mesozoic and cenozoic volcanic rocks in northeastern China. *Acta Pet. Sin.* 36, 324–336. (in Chinese with English abstract).

Yu, B., Li, W., Wang, X., and Yang, C. (2013). Tectonic evolution and its controlling on sedimentation in Hailar Basin. *Oil Geophys. Prospect.* 48, 289–296. (in Chinese with English abstract).

Zakaria, A. A., Johnson, H. D., Jackson, C. A.-L., and Tongkul, F. (2013). Sedimentary facies analysis and depositional model of the Palaeogene West Crocker submarine fan system, NW Borneo. *J. Asian Earth Sci.* 76, 283–300. doi:10.1016/j.jseaes.2013.05.002

Zeng, H., Ambrose, W. A., and Villalta, E. (2001). Seismic sedimentology and regional depositional systems in mioceno norte, lake maracaibo, Venezuela. *Lead. Edge* 20, 1260–1269. doi:10.1190/1.1487259

Zhang, T., Chen, J., Zhu, D., and Zhang, C. (2012). Origin of CO_2 gas from the north depression of the middle fault zone in the Hailar-Tamtsag Basin and natural gas in nearby depressions. *Chin. J. Geochem.* 31, 95–102. doi:10.1007/s11631-012-0554-6

Zhao, L. M., and Cui, R. F. (2014). Application of digital high-density seismic exploration in fine structural interpretation in coalfield. *Prog. Geophys.* 29 (5), 2332–2336.

Zheng, W., Hu, X., Chen, S., Liu, J., and Jia, C. (2016). The discovery and significance of a sedimentary hiatus within the carboniferous taiyuan formation, northeastern ordos basin, China: Discussion. *AAPG Bull.* 100, 1061–1066. doi:10.1306/12091515066

Zhou, Y., Ji, Y., Pigott, J. D., Meng, Q. A., and Wan, L. (2014). Tectono-stratigraphy of lower cretaceous tanan sub-basin, tamtsag basin, Mongolia: Sequence architecture, depositional systems and controls on sediment infill. *Mar. Petroleum Geol.* 49, 176–202. doi:10.1016/j.marpetgeo.2013.10.005